Recent Development of Lithium Borohydride-based Materials for Hydrogen Storage

*Wenxuan Zhang, Xin Zhang, Zhenguo Huang, Haiwen Li, Mingxia Gao, Hongge Pan, Yongfeng Liu**

W. X. Zhang, Dr. X. Zhang, Prof. M. X. Gao, Prof. H. G. Pan, Prof. Y. F. Liu
State Key Laboratory of Silicon Materials and School of Materials Science and Engineering, Zhejiang University, Hangzhou 310027, China
E-mail: mselyf@zju.edu.cn
Prof. H. G. Pan, Prof. Y. F. Liu
Institute of Science and Technology for New Energy, Xi'an Technological University, Xi'an, 710021, China
Prof. Z. G. Huang
School of Civil & Environmental Engineering, University of Technology Sydney, 81 Broadway, Ultimo, NSW, 2007, Australia
Prof. H. W. Li
Hefei General Machinery Research Institute, Hefei 230031, China

Keywords: hydrogen, hydrogen storage, borohydrides, $LiBH_4$, thermodynamics, kinetics

Abstract:

Lithium borohydride ($LiBH_4$) has been attracting extensive attention as an exemplary high-capacity complex hydride for solid-state hydrogen storage applications because of its high hydrogen capacities (18.5 wt% and 121 kg H_2 m^{-3}). However, the strong and highly directional covalent and ionic bonds within $LiBH_4$ structure induce high desorption temperatures, slow kinetics and poor reversibility, which make large-scale application impractical. To improve its hydrogen cycling performance, several strategies including cation/anion substitution, catalyst doping, reactive compositing and nanoengineering, have been developed to tailor the thermodynamics and kinetics of hydrogen storage process. For example, largely reduced operation temperatures and remarkably improved hydrogen storage reversibility under moderate conditions have been achieved by the synergistic effect of nanostructuring and nanocatalysis. Herein, the state-of-the-art development of $LiBH_4$-based hydrogen storage materials is summarized, including the basic physical and chemical properties, the principles of thermodynamic and kinetic manipulation and the straetegies to improve hydrogen storage properties. The remaining challenges and the main directions of future research are also discussed.

1. Introduction

The rapid development of human society has led to an ever-growing demand for energy and serious issuse such as climate change.[1] Hydrogen is considered as a clean energy carrier because it has the highest gravimetric energy density (142 MJ kg^{-1}) among all the typical energy fuels as well as being highly abundant, environmentally benign and renewable.[2] It is therefore expected in the future to replace the fossil fules used in industrial, residential and commercial sectors, including storing energy, generating electricity, cooking, and fuelling automobiles.[3] One of the most successful example is hydrogen-based fuel cell vehicles, which have been commercialized by Toyota, Hyundai, and Honda.[4] A variety of wind-hydrogen, solar-hydrogen, and solar-wind-hydrogen energy systems have been desgined and evaluated in Japan, USA, China, Canada, Germany, Norway, Greece, Spanish, etc.[5] However, the use of hydrogen as an energy carrier is faced with a tough problem since hydrogen is a gas at room temperature and atmospheric pressure, and its volumetric energy density is extremely low.[6] Traditionally, hydrogen can be stored as pressurized gas and cryogenic liquid.[7] Those processes can improve the density, but are extremely energy intensive. A safe, efficient and economic method for hydrogen storage and transportation is of critical importance.

Materials-based solid state hydrogen storage technique, in which hydrogen is bonded by either chemical or physical forces, has been becoming very attractive, thanks to their high gravimetric and volumetric storage capacities and safe operating pressures.[8] A wide variety of materials have been studied for hydrogen storage, including interstitial hydrides, binary hydrides, complex hydrides and adsorbents.[9] **Figure 1** shows the typical classification of solid hydrogen storage materials. Due to their high hydrogen capacity, complex hydrides are among the most studied.[10]

Complex hydrides represent a family of hydrides composed of metal cations and hydrogen-containing complex anions, in which hydrogen is covalently bound to a central atom.[11] With light weight and high hydrogen content, complex hydrides have attracted intense interests for

hydrogen storage applications. In particular, lithium borohydride ($LiBH_4$) has 18.5 wt% H, one of the most promising materials to meet the ultimate targets of on-board hydrogen storage for light-duty fule cell vehicles published by the US Deprtment of Energy.[12] However, the high desorption temperatures, slow kinetics, and poor reversibility caused by the strong and highly directional covalent and ionic bonds within $LiBH_4$ structure lead to unfavourable hydrogen cycling performance. Considerable work has been conducted to tackle these problems, and several strategies have been proposed and developed to tailor thermodynamics and kinetics of hydrogen storage process, including cation/anion substitution, catalyst doping, reactive compositing and nanoengineering. This review deals with the recent development of $LiBH_4$-based hydrogen storage materials, especially focusing on the strategies for thermodynamics and kinetics tailoring with the aim at improving hydrogen cycling performance.

2. Basic Physical and Chemical Properties of $LiBH_4$

$LiBH_4$ is a white solid at room temperature with a melting point of 278 °C and a density of 0.68 g/cm^3.[13] The standard formation enthalpy of $LiBH_4$ ($\Delta_f H^0$) is -190.8 kJ mol^{-1}.[14] It is soluble in some strong polar organic solvents, such as methyl tert-butyl ether, diethyl ether, tetrahydrofuran,[15] but reacts violently with H_2O to liberate H_2. $LiBH_4$ exists in four crystal polymorphs (**Figure 2**).[16] At room temperature, it is in the orthorhombic space group *Pnma*, in which each Li^+ ion is surrounded by four $[BH_4]^-$ tetrahedra and vice versa.[17] The tetrahedral $[BH_4]^-$ groups are aligned along two orthogonal directions with severe distortion in respect to bond lengths [*d*(B-H) = 1.04-1.28 Å] and angles (H-B-H = 85.1-120.1º) (**Figure 2**a). The lattice parameters are determined to be *a* = 7.18 Å, *b* = 4.43 Å and *c* = 6.80 Å. A phase transition occurs from orthorhombic to hexagonal (space group $P6_3mc$) upon heating to 108 ºC.[17] In the hexagonal phase, the tetrahedral configuration is adjusted and the $[BH_4]^-$ tetrahedra align along the *c*-axis with more symmetric arrangement. One $[BH_4]^-$ group is far away from Li^+, and one Li-B bond length becomes 3.11 Å while the other three shrinks to 2.55 Å (**Figure 2**b). After

being subjected to a pressure of 1.1-10 GPa at room temperature, $LiBH_4$ transforms into a new phase with pseudo-tetragonal structure (space group *Ama2*), which then changes to cubic phase (space group *Fm-3m*) above 10 GPa.[18] In *Ama2* phase, the $[BH_4]^-$ group presents a nearly square-planar coordination by four Li^+ ions (**Figure 2**c), while in the cubic phase the Li^+ ions and $[BH_4]^-$ groups are octahedrally coordinated (**Figure 2**d).

Historically, $LiBH_4$ was first synthesized from ethyl lithium (LiEt) and diborane in 1940 by Schlesinger and Brown as described below.[19]

$$LiEt + B_2H_6 \rightarrow LiBH_4 + BEtH_2 \quad (1)$$

Afterwards, they replaced LiEt by LiH by the following reaction.

$$LiH + \frac{1}{2}B_2H_6 \rightarrow LiBH_4 \quad (2)$$

Moreover, reacting LiH or $LiAlH_4$ with BF_3 etherate or alkylborates gives rise to $LiBH_4$ under the right conditions.[20]

$$4LiH + BF_3 \cdot Et_2O \rightarrow LiBH_4 + 3LiF + Et_2O \quad (3)$$

$$LiAlH_4 + B(OMe)_3 \rightarrow LiBH_4 + Al(OMe)_3 \quad (4)$$

Alternatively, $LiBH_4$ can be produced by direct reaction of Li metal or LiH with elemental B. The reaction conditions are very harsh because of the inertness of B (*T*: ~600-700 ºC, *p*(H_2): ~ 70-350 bar for LiH and B).[21]

$$LiH + B + \frac{3}{2}H_2 \rightarrow LiBH_4 \quad (5)$$

$$Li + B + 2H_2 \rightarrow LiBH_4 \quad (6)$$

Most practically, $LiBH_4$ is produced by the cation exchange reaction between LiCl(Br) and $NaBH_4$ in isopropylamine.[22]

$$LiCl(Br) + NaBH_4 \rightarrow LiBH_4 + NaCl(Br) \quad (7)$$

For large-scale applications, the cost of $LiBH_4$ needs to go down and a better synthetic method is needed.

3. Fundamentals of Hydrogen Storage in $LiBH_4$

For a long time, $LiBH_4$ was only used in chemical synthesis as a raw material for various organic redox processes and preparing other borohydrides.[15] In 2003, Züttel et al. reported hydrogen storage properties of $LiBH_4$ for the first time.[23] Their work stimulated intense interest in using borohydrides for hydrogen storage in the following two decades.

Considerable work has been conducted to understand the thermal decomposition behavior of $LiBH_4$. In general, $LiBH_4$ decomposes into LiH and B along with the release of H_2 upon heating as described below.[24]

$$LiBH_4 \rightarrow LiH + B + \frac{3}{2}H_2 \quad (8)$$

In fact, the thermal decomposition process of $LiBH_4$ is much more complicated with a multistep decomposition pathway as revealed by differential thermal analysis (DTA) studies.[25] Three main thermal events were detected in sequence while heating from room temperature to 600 ºC, including (1) a polymorphic phase transition at around 110 ºC; (2) the melting of $LiBH_4$ at around 278 ºC; and (3) decomposition into LiH and B with H_2 evolution at around 485 ºC, as summarized in **Figure 3**.[26] Recent reports also revealed the formation of B-containing intermediates, including $Li_2B_{12}H_{12}$ or $Li_2B_{10}H_{10}$, during thermal decomposition of $LiBH_4$.[27] In particular, Pitt et al. observed a new γ-$Li_2B_{12}H_{12}$ polymorph and a substoichiometric $Li_2B_{12}H_{12-x}$ intermediate with solid-state NMR and X-ray diffraction (XRD) analysis, and proposed the decomposition sequence of $LiBH_4$ as follows.[28] However, the exact decomposition mechanism of $LiBH_4$ is still not thoroughly understood so far.

$$12LiBH_4 \rightarrow \gamma - Li_2B_{12}H_{12} + 10LiH + 13H_2 \quad (9)$$

$$\gamma - Li_2B_{12}H_{12} \rightarrow Li_2B_{12}H_{12-x} + \frac{x}{2}H_2 \quad (10)$$

$$Li_2B_{12}H_{12} + 10LiH \rightarrow (12)a - BLi_{(y+2)/12} + (10-y)LiH + \frac{(12-x+y)}{2}H_2 \quad (11)$$

In theory, the hydrogen desorption of $LiBH_4$ is thermodynamically reversible because of the endothermic nature. The decompostion products LiH and B were rehydrogenated to yield $LiBH_4$ at 600 ºC and 350 bar H_2 or 727 ºC and 150 bar H_2.[26,29] The quite high hydrogenation temperatures likely originate from the inertness of elemental B, making it hard to form B-H bonds. Therefore, tailoring thermodynamics and kinetics is of critical importance for improving hydrogen storage properties of $LiBH_4$, especially for reducing the operating temperatures and speeding up the reaction rates.

4. Tailoring Thermodynamics and Kinetics for Hydrogen Storage in $LiBH_4$

The typical reaction between hydrogen and materials involves the adsorption and absorption of H_2 molecules, the breaking of H-H bonding, the diffusion of H atoms, and the formation of X-H (X=metal, boron, etc) bonds. In a typical reversible hydride, the hydrogen atoms are stored in interstices of structures or chemically bonded to the central elements. The hydrogen is detached by changing the thermodynamic conditions, for example, decreasing system pressure or increasing operating temperature. Here, the operating temperatures for hydrogen storage strongly depend on the thermal stability of hydrides and the kinetic energy barriers. To combine with PEMFCs, hydrogen storage systems are preferable to work below 80 ºC.[12] However, $LiBH_4$ starts releasing H_2 above 300 ºC even under vacuum, which is too high for practical application. To reduce the operating temperature, numerous efforts have been devoted to tailoring the thermodynamics and kinetics for hydrogen storage in $LiBH_4$. In the following parts, we summarize in detail the recently developed strategies for tailoring thermodynamics, kinetics,

and both of them, including cation/anion substitution, catalyst doping, reactive compositing and nanostructuring, as displayed in **Figure 4**.

4.1 Tailoring Thermodynamics for Hydrogen Storage in $LiBH_4$

From the thermodynamics point of view, the reaction temperature for hydrogen release from a metal hydride is mainly determined by the enthalpy change (ΔH) as described by the Gibbs free energy equation, since the entropy change (ΔS) is often considered to be a constant, which mainly originates from the gaseous hydrogen. Therefore, a feasible approach to reduce the desorption temperature is to decrease the ΔH values, which can be enabled by the destabilization of borohydrides or the stabilization of the decomposition products (**Figure 5**).[30]

The partial substitution of cations or anions is a frequently used strategy to thermodynamically destabilize metal borohydrides. A series of bimetallic or eutectic borohydrides have been prepared and characterized by combining $LiBH_4$ with other metal borohydrides (e.g., $NaBH_4$, KBH_4, $Mg(BH_4)_2$, $Ca(BH_4)_2$, $Zn(BH_4)_2$, $Sc(BH_4)_3$, $Zr(BH_4)_4$).[31] The reported bimetallic borohydrides include $LiZr(BH_4)_5$, $Li_2Zr(BH_4)_6$, $LiK(BH_4)_2$, $LiSc(BH_4)_4$, $LiZn_2(BH_4)_5$.[31a,31c,32] An eutectic phenomenon between $LiBH_4$ and $Mg(BH_4)_2$ was experimentally disclosed, which allows the release of hydrogen at a temperature lower than that of their individual component.[31f] The $Li_{1-x}Mg_{1-y}(BH_4)_{3-x-2y}$ displayed a largely decreased thermal stability and a distinctly different decomposition behavior from pristine $LiBH_4$.[31g] The melting point of the $0.725LiBH_4$-$0.275KBH_4$ system was even reduced to 105 °C along with the concurrence of dehydrogenation.[33] For the $x LiBH_4$+$(1-x)Ca(BH_4)_2$ system, reduced desorption temperatures were observed while x = 0.6-0.8.[34] The partial replacement of H^- ions by F^- ions also successfully reduced the decomposition temperature of $LiBH_4$ as demonstrated by Yin et al.[35] With the replacement of H^- ions, the decomposition enthalpy of $Li[BH_{4-x}]F_x$ could be reduced to 36.5 kJ mol^{-1} H_2, and the onset dehydrogenation temperature was redcued to 100 °C. The decomposition of $LiBH_3F$ commenced even at a lower temperature of ~80 °C.[36]

By mixing $LiBH_4$ with TiF_3 and $TiCl_3$, respectively, Fang et al. revealed that the substitution of F^- ions for H^- ions was much more effective in the reduction of desorption temperature than Cl^-.[37] In contrast, partially replacing BH_4^- in $LiBH_4$ with Br^- gave rise to the formation of a more stable *h*-$Li(BH_4)_{0.5}Br_{0.5}$ phase.[38] In addition, mixing $LiBH_4$ with $NH_3{\cdot}BH_3$ to form a new $LiBH_4{\cdot}NH_3BH_3$ complex also reduced the phase transformation enthalpy by 18%, and the hydrogen desorption capacity reached 15.7 wt% in the temperature range of 100-450 ℃, which is remarkably superior to pristine $LiBH_4$.[39] However, the reversibility of hydrogen storage has not been improved by partial substitution.

Alternatively, stabilization of the dehydrogenation products is also highly effective approach for tailoring the thermodynamics of hydrogen storage in $LiBH_4$. In this concept, $LiBH_4$ combines with reactive additives to form metal borides rather than elemental B after dehydrogenation, which reduces the overall desorption enthalpy change and increases the desorption equilibrium pressure, consequently reducing the operating temperature and improving the reversibility of hydrogen storage.[40] This was first demonstrated by Vajo et al. in 2005.[41] They observed the full reversibility of $LiBH_4$ while coupled with MgH_2 at a stoichiometric molar ratio (2:1) under relative mild conditions (< 450 ºC). The overall reaction process is expressed as follows.

$$2LiBH_4 + MgH_2 \leftrightarrow 2LiH + MgB_2 + 4H_2 \qquad (12)$$

Here, the formation of MgB_2 induced a reduction of 25 kJ mol^{-1} H_2 in the desorption enthalpy change with respect to pure $LiBH_4$, and the desorption temperature was decreased to 225 ºC at 1 bar of equilibrium pressure. Mechanistic investigation revealed a stepwise reaction process upon heating, where MgH_2 first decomposed into H_2 and Mg, which then reacted with $LiBH_4$.[42] After that, a variety of reactive destabilization systems were developed, including $LiBH_4$/Mg, $LiBH_4$/Al, $LiBH_4/CaH_2$, $LiBH_4/ScH_2$, $LiBH_4/CeH_2$, $LiBH_4/YH_3$, $LiBH_4/LaH_3$, $LiBH_4/Mg_2NiH_4$, $LiBH_4/Mg_2FeH_6$, $LiBH_4/Li_3AlH_6$, $LiBH_4/LiAlH_4$, $LiBH_4/Mg(AlH_4)_2$, and

$LiBH_4/Ca(AlH_4)_2$.[43] **Table 1** lists their hydrogen storage parameters. Yang et al. compared the destabilization effects of various metals and metal hydrides, including Al, Mg, Ti, Sc, V, Cr, MgH_2, CaH_2 and TiH_2, based on thermodynamics predicted by first-principles calculations.[43b,43c] Metal borides were detected after dehydrogenation for MgH_2, Mg, Al, and CaH_2 systems. Furthermore, it was found that the $2LiBH_4$/Al system stored reversibly 8.5 wt% H at 400-450 ºC with 38.2 kJ mol^{-1} H_2 of enthalpy change.[43d] The $LiBH_4/LiAlH_4$ combination liberated 8.7 wt% H at 500 ºC.[43e] A reversible hydrogen capacity of ~9.0 wt% was measured for $6LiBH_4/CaH_2$ system at 400 °C and 83–100 bar H_2 pressure with a reaction enthalpy change ranging from 40.7 to 60.2 kJ mol^{-1} H_2.[43f] By combining $LiBH_4$ with MgH_2 and CaH_2 together, the ending temperature for hydrogen release was further reduced by 160 ºC.[44] Similarly, a mixture of $LiBH_4$, $LiAlH_4$ and MgH_2 delivered 7.62 wt% of hydrogen capacity at 280 °C with good reversibility.[43g] The $LiBH_4/Mg_2NiH_4$ composite started releasing hydrogen from 250 ºC, thanks to the significantly low enthalpy (ΔH ~ 15.4 kJ mol^{-1} of H_2) and entropy (ΔS ~ 62.2 J/K mol^{-1} H_2).[45] At 270 ºC, a direct reaction between solid $LiBH_4$ and Mg_2NiH_4 was observed, leading to the formation of a ternary boride phase $MgNi_{2.5}B_2$.[46] This mechanism is distinctly different from the well-known $2LiBH_4$-MgH_2 system as discussed above.[42] For $2LiBH_4/Mg_2FeH_6$ system, however, an increased entropy change (147 J K^{-1} mol^{-1} H_2) was observed, which is responsible for improved thermodynamic properties.[43h] Gao et al. reported a $2LiBH_4$-$2MgH_2$-$Ca(BH_4)_2$ ternary system which started to release hydrogen from 320 ºC and completed at 370 ºC with ca. 8.1 wt% H capacity.[47] For the $LiBH_4$-$NaBH_4$-$Mg(BH_4)_2$ ternary system, hydrogen release occurred at 276 and 365 °C (peak temperature).[48] Ismail et al. reported a component conversion from $NaAlH_4$-MgH_2-$LiBH_4$ to $LiAlH_4$-MgH_2-$NaBH_4$ after ball milling.[49] Similar phenomenon was also observed for the Na_3AlH_6-$LiBH_4$ and MgH_2-Na_3AlH_6-$LiBH_4$ systems.[50] The $2LiBH_4$-$Mg(AlH_4)_2$ combination gave off 10.8 wt% H below 400 ºC with an onset temperature as low as 60 ºC.[43i] Recently, Bi_2Te_3 was used as a new

destabilizing agent to form the $LiBH_4$–Bi_2Te_3 composite, which started desorbing hydrogen at 61 °C with a total hydrogen capacity of 9 wt%.[51]

Unlike the above reactive hydride composites, $LiBH_4$ can also be destabilized by combining with $LiNH_2$ to form new quaternary hydrides, i.e., $Li_3BN_2H_8$ and $Li_4BN_3H_{10}$.[52] Moreover, the ammoniate of $LiBH_4$ released 17.8 wt% H in a closed system at 135-250 ºC.[53] The largely reduced desorption temperature was mainly attributed to the strong affinity between protonic $H^{\delta+}$ and hydridic $H^{\delta-}$. Unfortunately, the release of NH_3 by-product and the exothermic nature are quite unfavorable for practical applications. Introducing MgH_2 to form $LiBH_4$-$LiNH_2$-MgH_2 composite partially addressed these issues.[54] Based upon what has been reported so far, novel strategies involving more effective destabilizing agents are needed to further improve the hydrogen cycling property of $LiBH_4$.

4.2 Reducing Kinetic Barriers for Hydrogen Storage in $LiBH_4$

In addition to thermodynamics, the operating temperature for a hydrogen storage material is also closely related to the kinetic barriers, which control the reaction rate of hydrogen release and uptake. In comparison with traditional interstitial metal hydrides, the kinetic barriers for hydrogen storage in complex hydrides are usually much higher because of the low catalytic activity of constituent elements for the dissociation and reformation of H-H bonding and the complicated reaction pathways, especially for $LiBH_4$. Adding catalysts and nanostructuring have been proven to be effective in reducing kinetic energy barriers for hydrogen storage reaction of $LiBH_4$.

4.2.1 Catalytic Additives

Catalyst enables fast and effective dissociation of hydrogen molecules on the materials' surface, which is of critical importance for improving kinetics of hydrogen storage in hydrides. **Table 2** summarizes some typical catalytic additives and their effects. At first, investigations were mainly focused on metal oxides and halides.[23,55] Züttel et al. first evaluated the catalytic

effectiveness of SiO_2 and found that 25 wt% SiO_2-containing $LiBH_4$ released hydrogen from 200 ℃.[23] Yu et al. reported the catalytic activity of several transition metal oxides for hydrogen desorption from $LiBH_4$ in the order: Fe_2O_3>V_2O_5>Nb_2O_5>TiO_2>SiO_2.[55a] The onset dehydrogenation temperature of Fe_2O_3-catalyzed $LiBH_4$ (mass ratio: 2:1) was only 100 °C. Au et al. studied the effects of a series of metal halides such as $TiCl_3$, TiF_3 and ZnF_2.[55b] Approximately 3.5 wt% of H was released from $LiBH_4$-0.1TiF_3 at 150 ℃, which was further increased to 8.5 wt% at 450 ℃. Unfortunately, the evolution of the B_2H_6 impurity was also increased. A much superior catalytic activity was obtained for TiF_4 since the TiF_4-modified $LiBH_4$ released 6.3 wt% H at 150 ℃.[56] This result indicates that the high-valence Ti compounds are much more effective. Moreover, the addition of $FeCl_2$ and $NiCl_2$ induced the liberation of all hydrogen in $LiBH_4$. Their borides were believed to be the catalytic species and facilitated hydrogen release process.[55c] Similarly, the halides of rare earth metals also presented catalytic activity to some extent.[55d] The dehydrogenation temperatures were reduced to 220-320 ℃ with the presence of $CeCl_3$ or $LaCl_3$. The Ce-based halides were much superior to those of La. The metallic Ni-doped $LiBH_4$ system released the majority of hydrogen below 600 ºC, and achieved the partial hydrogenation at 600 ºC and 100 atm.[55e] The hydrogenation pressure was largely reduced. Xu et al. successfully prepared 9.7 nm-sized Ni supported on graphene (Ni/G) by using a hydrogen thermal reduction method, which exhibited superior catalytic activity for hydrogen storage in $LiBH_4$.[57] Adding 20 wt% Ni/G induced hydrogen desorption from $LiBH_4$ starting at 180 °C and around 12.8 wt% of H was desorbed within 45 min at 450 °C. More importantly, the hydrogen capacity stabilized at 9.8 wt% at 400 °C and under 30 bar H_2 after 30 cycles. Meng *et al*. reported similar results using well-dispersed Ni nanoparticles supported by porous carbon as catalytic additives.[58] Further first-principles calculations revealed that transition metal modification decreased the hydrogenation removal energy during the H atom release process from the bulk, therefore favoring hydrogen desorption.[59] The Ti-doped $LiBH_4$ was demonstrated to have a good dehydrogenation

performance. Two dimensional layered MXene Ti_3C_2, nanosized Ce_2S_3, and $NiFe_2O_4$ were also used to improve hydrogen storage properties of $LiBH_4$.[60] The onset dehydrogenation temperature of 40 wt% Ti_3C_2-containing $LiBH_4$ was 120 ºC and approximately 5.37 wt% hydrogen could be liberated within 1 h at 350 ºC with a largely reduced activation energy (70.3 kJ mol^{-1} H_2).[60a] The initial dehydrogenation temperature of the $LiBH_4$-20 wt% Ce_2S_3 composite was decreased to 250 °C, and the release of hydrogen reached 4 wt% within 3000 s at 400 °C, which is 1.67 times higher than that of pristine $LiBH_4$.[60b] As for nanosized $NiFe_2O_4$, a 9 mol% addition reduced the onset and peak dehydrogenation temperature to 89 °C and 190 °C, respectively, lowered by 226 °C and 260 °C relative to pristine $LiBH_4$.[60c]

In addition, carbon-based materials, including activated carbon, carbon nanotubes, graphene, g-C_3N_4, etc., have also attracted considerable attentions for catalyzing hydrogen desorption from $LiBH_4$. A 30 wt% SWCNTs-modified $LiBH_4$ ball milled for 1 h started to decompose around 280 °C, which is about 150 °C lower than that of pristine $LiBH_4$ treated under identical conditions, and hydrogen desorption reached 12.3 wt% while heating to 550 ºC.[61] SWNTs and activated carbon were found to have better catalytic effects on the hydrogen storage properties of $LiBH_4$ than graphite.[62] A reduction of 60 ºC in the onset desorption temperature was observed for MWCNTs-modified $LiBH_4$.[63] Similarly, with the addition of C_{60}, the dehydrogenation temperature of $LiBH_4$ was lowered to ~320 °C.[64] The presence of 20 wt% graphene reduced the onset dehydrogenation temperature of $LiBH_4$ to 195 ºC, and the peak temperature to 300 ºC.[65] The addition of 3D porous fluorinated graphene enabled a fast and successive dehydrogenation process at 305 °C, which is much lower than pure $LiBH_4$.[66] Theoretical predication revealed that C_3N_4 was a potential dehydrogenation catalyst for $LiBH_4$.[67] This was experimentally evidenced in the $LiBH_4$-MgH_2 system as the apparent activation energy was reduced from ~ 200 kJ mol^{-1} H_2 to 126 kJ mol^{-1} H_2 with the introduction of Ni@g-C_3N_4.[68]

Recently, investigations on catalyst-modified $LiBH_4$ were expanded to organic materials. The onset temperature of hydrogen desorption from a 20 wt% polyaniline-containing $LiBH_4$ was as low as 75 ℃, and the hydrogen capacity remained at 3.9 wt% after 5 cycles. Mechanistic studies revealed that upon dehydrogenation, the oxygen-containing groups of polyaniline reacted with $LiBH_4$ to generate Li_3BO_3 and $LiBO_2$, which exhibited a good catalytic effect on $LiBH_4$.[69] This was further proven by Li *et al*.[70] By using niobium ethoxide as the precursor, Li_3BO_3 and NbH were *in situ* formed by reacting with $LiBH_4$ upon heating. The introduction of Li-B-O compounds reduced the onset dehydrogenation temperature to 200 °C, and the hydrogen capacity retention was determined to be as high as 91% after 30 cycles. This sufficiently indicates the effectiveness of the Li-B-O compounds in catalyzing the hydrogen storage process of $LiBH_4$.

In general, highly active catalysts can effectively enhance the reaction rate for hydrogen storage in hydrides, even added in small amounts. As for $LiBH_4$, however, the amount of catalytic additives is often higher than 10 wt%, even up to 50 wt%. In addition, most reported catalytic additives reacted with $LiBH_4$ forming new compounds, which makes the actual catalytically active species unclear. The corresponding catalytic mechanisms therefore remain elusive. Further efforts should be devoted to finding out the real mechanims, which will help to develop more effective catalysts.

4.2.2 Nanostructuring or Nanoconfinement

Reducing particle size has been frequently used to improve hydrogen storage kinetics of hydrides, especially for complex hydrides, owing to largely increased surface area and shortened diffusion distances, which enables a low kinetic barrier for hydrogen absorption and desorption.[71] Due to the strong reducing capability and complicated elemental composition, it is quite difficult to synthesize the isolated complex hydride in nanoscale, especially for $LiBH_4$. Several unique preparation processes have been developed for this purpose.[72] In 2014, Pang

and co-workers proposed a novel mechanical-force-driven physical vapour deposition method.[72a] By using $[LiBH_4(MTBE)]_n$ (MTBE: methyl tert-butyl ether) as the precursor, $LiBH_4$ nanobelts with widths of 10-40 nm were successfully synthesized, which showed significantly lowered dehydrogenation temperature as measured by TPD-MS (**Figure 6**). With a solvent evaporation strategy, Li *et al*. obtained $LiBH_4$ nanoparticles with sizes ranging from 10.6 to 147.4 nm, stabilized by poly(methl methacrylate).[72b] The particle sizes depended on the concentration of $LiBH_4$ in tetrahydroguran (THF). Wang *et al*. reported that the binding force between the surfactant and $LiBH_4$ controlled the growth and stabilization of $LiBH_4$ nanoparticles.[72c] By reacting diborane (B_2H_6) with nanosized-LiH obtained via thermal decomposition of alkyllithium, $LiBH_4$ nanoparticles were successfully fabricated.[72d] B_2H_6 is highly toxic and flammable so it is better to develop different methods of synthesis. Antisolvent precipitation or solvent displacement proved effective in preparing $LiBH_4$ nanoparticles with a relatively good distribution of particle size.[72e] For most of methods reported, however, suitable stabilizing agents are essential and their complete removal is an issue.

Nowadays, a more common approach to prepare nanosized $LiBH_4$ is nanoconfinement, where $LiBH_4$ was confined into a porous host material. **Table 3** summarizes hdyrogen storage properties of representative nanoconfined $LiBH_4$ systems. In 2008, Gross *et al*. successfully confined $LiBH_4$ into pyrolyzed resorcinol-formaldehyde aerogels with pore sizes of 13 and 25 nm by means of melt infiltration.[73] This induced a remarkable reduction in the activation energy from 146 to 103 and 111 kJ mol^{-1}, respectively. After that, Cahen *et al*. loaded 33 wt% $LiBH_4$ into 4 nm-sized mesoporous carbon by solution impregnation in ethers.[74] Nanosized $LiBH_4$ displayed a single desorption peak at 200-300 ºC, 100 ºC lower than that of bulk counterpart. Christian *et al*. deposited $LiBH_4$ nanoparticles on carbon nanotubes, which reduced the desorption activation energy even to 88 kJ mol^{-1} H_2.[75] Liu *et al*. observed a reduction of 240 ºC in the onset desorption temperature after confining $LiBH_4$ into highly ordered hexagonally packed cylindrical nanoporous carbon (NPC) with an average pore size of 2 nm.[76]

When the pore size was below 4 nm, the phase transition and melting of nanoconfined $LiBH_4$ were invisible upon heating.[77] Using activated carbon nanofiber prepared from polyacrylonitrile as the host for nanoconfined $LiBH_4$, reduction in onset and main dehydrogenation temperatures (ΔT = 128 and 118 °C, respectively) together with suppression of B_2H_6 release were achieved simultaneously.[78] Gausalawit-Utke *et al*. reported that confining $LiBH_4$ in poly(methyl methacrylate)–co–butyl methacrylate ($LiBH_4$–PMMA–co–BM) reduced the hydrogen desorption temperature of $LiBH_4$ to 80 ºC, and the amount of hydrogen released reached 8.8 wt% H at 120 ºC after 2h, while no hydrogen release was detected for pristine $LiBH_4$ under the same conditions.[79] Moreover, nano $LiBH_4$–PMMA–co–BM can be partially hydrogenated at 140 °C under 50 bar H_2 for 12 h. $LiBH_4$ confined in porous hollow carbon nanospheres released rapidly 8.1 wt% H at 350 ºC within 25 min.[80] Using copper-metal–organic frameworks as the host, Sun *et al*. reduced the desorption temperature of $LiBH_4$ to 75 ºC with the peak temperature at 110 °C, and observed an interaction between $LiBH_4$ and Cu^{2+} ions.[81] By encapsulating $LiBH_4$ in carbon nanocages, hydrogen desorption temperature was reduced to 320 °C with an 200 °C onset temperature and rehydrogenation was obtained under 400 °C and 50 bar H_2.[82] By using zeolite-templated carbon as a host material, Shao *et al*. detected hydrogen desorption at 194 ºC for $LiBH_4$, which is 181 ºC lower than that of the bulk sample.[83] Sun *et al*. even observed the release of 8.5 wt% H from $LiBH_4$ confined by SBA-15 within 10 min at 105 ºC.[84] However, the reversibility of hydrogen storage was lost because no hydrogen uptake was found at 450 °C under 70 bar H_2. Recently, a unique double-layered carbon nanobowl-confined $LiBH_4$ composite with 80 wt% of loading was successfully prepared by melt infiltration, which readily desorbed and absorbed ~8.5 wt% of H at 300 °C and under 100 bar H_2 (**Figure 7**).[85] Alternatively, porous TiO_2 tubes, CuS nanospheres, $NiMnO_3$ nanospheres, hierarchical $ZnO/ZnCo_2O_4$ nanoparticles and 2D Ti_3C_2 were also used as host materials to confine $LiBH_4$.[79,86] With porous TiO_2 micro-tubes as the host (**Figure 8**), the nanoconfined $LiBH_4$ started releasing hydrogen at 180 °C, and the apparent activation

energy was reduced to 121.9 kJ mol^{-1} H_2.[86a] Hollow and porous CuS led to 40 °C of onset desorption temperature and 100 °C of peak temperature, but only 0.6 wt% of H was reversible at 300 ºC under 60 bar H_2.[79] The confinement of $LiBH_4$ in porous $NiMnO_3$ nanoparticles led to the release of hydrogen at 150 °C and the peak desorption temperature was 300 °C.[86b] The peak desorption temperature was reduced to 275 °C for $LiBH_4$ confined in hierarchical porous $ZnO/ZnCo_2O_4$ nanoparticles, and 8.7 wt% H was liberated below 500 °C.[86c] With a novel wet chemical process, Xia *et al*. obtained graphene-supported $LiBH_4$ nanolayers with a thickness of 4 nm, which showed a fast dehydrogenation at 340 ºC with a capacity of 9.7 wt%.[87] In particular, the hydrogen capacity of graphene-supported $LiBH_4$ nanolayers remained at 7.5 wt% after 5 cycles at 320 ºC, corresponding to a capacity retention of 80%, which was nearly twice that of $LiBH_4$/G mixture after 3 cycles (**Figure 9**).

Although significant progress has been made in nanoconfined $LiBH_4$ for reversible hydrogen storage, the chemical inertness of host materials and low loading efficiency induce a penalty in gravimetric hydrogen capacity, sometimes making it even lower than that of traditional interstitial metal hydrides. In addition, the local confinement environments make it challenging to characterize the size effect. In these regards, the development of light-weight host materials and increasing effective loading should be emphasized. At the same time, a controllable fabrication of stable, support-free nanostructured $LiBH_4$ should be explored.

4.3 Simultaneously Tailoring Thermodynamics and Kinetics

Simultaneous adjustment of thermodynamics and kinetics is a key route to decrease the operating temperatures and enhance the reaction kinetics for hydrogen storage in $LiBH_4$. The most frequently used approach is introducing catalysts into reactive composites and nanoconfined systems. Nanoconfinement of reactive composites and mixed borohydrides is also an option. Considerable work has been conducted in recent years.

4.3.1 Catalyst Doping into Reactive Composites

The $2LiBH_4$-MgH_2 combination is a typical thermodynamically destabilized system. To further enhance the hydrogen storage reaction kinetics, various catalytic additives were introduced into this system, including carbon materials, metals (Pd, Ni, Ru, Fe), metal halides ($TiCl_3$, TiF_3, $ZrCl_4$, $CuCl_2$, $HfCl_4$, VCl_3, NbF_5), metal oxides (Nb_2O_5, Sc_2O_3, Fe_2O_3, MgO) and metal borides (MgB_2, TiB_2, NbB_2). In 2005, Vajo *et al*. reported that $2LiBH_4$-MgH_2-3 mol% $TiCl_3$ composite delivered reversible hydrogen capacity of 8-10 wt% at 315-450 ºC.[41] Increasing $TiCl_3$ to 5 mol%, the onset desorption temperature was further decreased to 240 ºC.[88] Compared with $FeCl_2$ and $CoCl_2$, $NiCl_2$ is the best catalyst because of the formation of $MgNi_3B_2$ which worked as the nucleation site for MgB_2.[89] Compared with TiF_3, CeF_3, LaF_3 and FeF_3, NbF_5 presented the best catalytic activity due to the its reaction with $LiBH_4$ and the $0.05NbF_5$-containing $2LiBH_4$-MgH_2 system desorbed 8.1 wt% H below 450 ºC.[90] Furthermore, Mao *et al*. reported that NbF_5 suppressed the formation of $Li_2B_{12}H_{12}$.[91] The influence of $MoCl_3$ was also investigated, which led to a capacity of about 7 wt% hydrogen at 300 ºC.[92] The highly dispersed metallic Mo formed by the reaction with $LiBH_4$ was the reason for the improved hydrogen storage performance. In TiF_3 and TiF_4-modified systems, TiB_2 was identified as nucleation agents for the formation of MgB_2 during dehydrogenation.[93] Fan *et al*. found that amorphous TiB_2 and NbB_2 nanoparticles significantly improved the hydrogen storage performance of the $2LiBH_4$-MgH_2 system.[94] Zhao *et al*. observed the release of 10.8 wt% H from CoNiB-catalyzed $2LiBH_4$-MgH_2 system below 500 ºC.[95] The use of $CuCl_2$ as a catalytic additive in $2LiBH_4$-MgH_2 gave rise to the formation of Mg-Cu alloy, which promoted the nucleation of MgB_2 by working as heterogeneous nuclei.[96]

The introduction of Pd nanoparticles into $2LiBH_4$-MgH_2 resulted in 80 ºC of reduction in the initial dehydrogenation temperature from 340 to 260 ºC and the total hydrogen capacity was determined to be 8.0 wt% below 400 ºC.[97] Mg_6Pd was detected after dehydrogenation. Approximately 7.9 wt% hydrogen was recharged into the dehydrogenated product at 400 ºC and under 35 atm H_2 for 6 h. The Ru/C-doped $2LiBH_4$–MgH_2 sample liberated 8.39 wt% H

within 2 h at 380 °C, while only 6.37 wt% hydrogen was released for the undoped sample even after 5 h.[98] The addition of Fe lowered the onset decomposition temperature by 30 ºC and led to considerably faster isothermal dehydrogenation during the first cycle, thanks to the formation of nanocrystalline, well distributed FeB.[99] The dehydrogenation temperature of Ti-containing $2LiBH_4$-MgH_2 system was 50-70 ºC lower than that of the additive-free system.[100] Fan *et al*. revealed the catalytic effect of Nb_2O_5 on reversible hydrogen storage performances of $2LiBH_4$-MgH_2 composite,[101] which released approximately 6–8 wt% below 400 ºC and stabilized at 5.16 wt% after 3 cycles. Compared with pure $2LiBH_4$-MgH_2 composite, the addition of 10 mol% MgB_2 reduced the hydrogenation time to only half, which was further shortened to about one-fifth for 5 mol% Sc_2O_3.[102] The presence of Li_xTiO_2 led to the direct formation of MgB_2 by suppressing the formation of $Li_2B_{12}H_{12}$ intermediate, consequently speeding up the first dehydrogenation.[103] By co-doping Fe_2O_3 and TiF_3, the onset desorption temperature of $2LiBH_4$-MgH_2 composite was reduced to 110 ºC.[104] With $BaTiO_3$ as an additive, the onset dehydrogenation temperature was decreased by 124 ºC.[105] Upon dehydrogenation, $BaTiO_3$ reacted with $LiBH_4$ forming BaB_6 and TiO_2. BaB_6 is beneficial to lower the stability of $LiBH_4$, while TiO_2 has a catalytic effect in improving the kinetics of hydrogenation/dehydrogenation. Titanium isopropoxide could significantly improve the kinetics of the $2LiBH_4$–MgH_2 system.[106] Mechanistic investigation revealed that the high dispersion of titanium-based additives resulted in a distinct grain refinement of MgB_2 and an increase in the number of reaction sites, which is responsible for the accelerated desorption and absorption.[107]

An average dehydriding rate over 2 times faster than that of the neat $LiBH_4$/MgH_2 sample at 450 ºC was obtained after adding 10 wt% SWNTs.[108] A rapid hydrogen desorption was also observed for activated carbon-modified $2LiBH_4$-MgH_2 composite due to the tailored nanophase structure.[109] The pre-milled MWCNTs induced a reduction of 50 ºC in dehydrogenation temperature.[110] Further improvement of desorption kinetics was achieved after adding CNT into the Ni-catalyzed $2LiBH_4$-MgH_2 system.[111] By doping with 15 wt% MWCNTs-TiO_2,

compacted $2LiBH_4$-MgH_2 delievered gravimetric and volumetric hydrogen storage capacities of 6.8 wt% and 68 g H_2 L^{-1}, respectively.[112] Co and Ni-based catalysts improved hydrogen cycling performance of binary $LiBH_4$-$Mg(BH_4)_2$ and $LiBH_4$-$LiNH_2$ systems, respectively.[113] Although hydrogen desorption temperatures were largely lowered with the presence of catalytic additives (**Table 4**), the reversibility of hydrogen storage in these binary systems has not been improved effectively, which is critical for practical applications.

4.3.2 Nanostructuring of Thermodynamically Destabilized Systems

Nanoconfinement was also employed to improve hydrogen storage properties of some reactive composites and mixed borohydrides, including $LiBH_4$-MgH_2, $LiBH_4$-Mg_2NiH_4, $LiBH_4$-$LiAlH_4$, $LiBH_4$-$NaAlH_4$, $LiBH_4$-MgH_2-$NaAlH_4$, $LiBH_4$-$NaBH_4$ $LiBH_4$-KBH_4, $LiBH_4$-$Mg(BH_4)_2$, and $LiBH_4$-$Ca(BH_4)_2$. **Table 5** summarizes hydrogen storage properties of these modified systems. In 2010, Nielsen *et al*. successfully confined $LiBH_4$ and MgH_2 nanoparticles in a nanoporous carbon aerogel scaffold with a pore size of ~ 21 nm by a stepwise synthesis process.[114] The nanoconfined system showed rapid hydrogen desorption and a high degree of reversibility. 74% of the total hydrogen content in nanoconfined $2LiBH_4$-MgH_2 was released below 320 ºC, but it was only 26% for the bulk sample. By direct melt infiltration of bulk $2LiBH_4$-MgH_2 into a nanoporous resorcinol-formaldehyde carbon aerogel scaffold, Gosalawit-Utke *et al*. observed the release of 90% of the total hydrogen storage capacity within 90 min at 425 ºC.[115] The activation energy of the decomposition of $LiBH_4$ and MgH_2 was decreased by 27 and 132 kJ mol^{-1} H_2, respectively, due to nanoconfinement, and the calculated enthalpy changes were in the range of 46.21 kJ mol^{-1} H_2.[116] By pre-milling MgH_2, Gosalawit-Utke *et al*. obtained a dehydrogenation rate approximately twice faster for the nanoconfined sample than that of the sample without MgH_2 pre-milling.[117] With a self-assembly followed by solution infiltration, Xia and coworkers fabricated a graphene-supported monodispersed $2LiBH_4$-MgH_2 nanocomposite with a particle size of ~ 10.5 nm. The nanostructuring largely facilitated the physical contact between $LiBH_4$ and MgH_2 and shortened the mass transport distance, which

induced a reversible storage capacity of up to 8.9 wt% at 350 ºC.[118] Recently, a novel ball milling process fitted with aerosol spraying was used to fabricate a mixture of nano-$LiBH_4$ and nano-MgH_2, which delievered 5 wt% of reversible storage capacity at temperatures ≤ 265 ºC.[119] A nanoconfined $LiBH_4$-Mg_2NiH_4 showed a single-step reaction at around 300 ºC with 4.2 wt% of hydrogen capacity.[120] The main dehydrogenation temperature of the nanoconfined $LiBH_4$-$LiAlH_4$ was reduced by 94 ºC when compared with the milled sample.[121] Nanoconfinement of $2LiBH_4$-$NaAlH_4$ enabled an onset of hydrogen release below 100 ºC, which was 132 ºC lower than that of bulk system.[122] For the ternary system of $LiBH_4$-MgH_2-$NaAlH_4$, nanoconfinement not only converged multiple-step decomposition into a single step but also largely reduced the dehydrogenation temperature, approximately by 70 ºC regarding the last dehydrogenation step.[123]

The hydrogen storage properties of eutectic mixed borohydride systems were also significantly improved by nanoconfinement. The first report on the nanoconfinement effect of a binary borohydride mixture co-infiltrated into mesoporous scaffolds was made by Lee *et al*. in 2011.[124] They infiltrated the eutectic $LiBH_4$–$Ca(BH_4)_2$ composite into the mesoporous channels of the carbon by melt infiltration and observed that the major dehydrogenation event occurred at ~300 °C, which is lower compared with the same composite without carbon. After infiltration, $LiBH_4$ and $Ca(BH_4)_2$ existed as an amorphous mixture inside the pores and there was a certain interaction with the mesoporous scaffolds, which likely contributed to a faster dehydrogenation.[125] The CO_2-activated carbon aerogel scaffold was more inert and enabled faster kinetics and higher stability for the $LiBH_4$–$Ca(BH_4)_2$ eutectic system.[126] Similar phenomenon was also observed in the $LiBH_4$-$NaBH_4$ and $LiBH_4$-KBH_4 systems.[33,127] The CO_2-activated carbon aerogel-confined $0.62LiBH_4$–$0.38NaBH_4$ maintained ~70% of the initial capacity after 4 cycles, more than 3-fold that of bulk mixture.[127] As for $0.725LiBH_4$-$0.275KBH_4$, nanoconfinement lowered the main hydrogen release temperature by up to 200 ºC in the first cycle.[33,128] Nanoconfinement of $0.55LiBH_4$–$0.45Mg(BH_4)_2$ in high surface area

carbon aerogel led to a favorable hydrogen release as illustrated by the release of 7.62 wt% H from room temperature to 500 ºC.[129] More than 10.8 wt% hydrogen (referred to borohydride) was released from porous hollow carbon nanospheres-confined $LiBH_4$-$Mg(BH_4)_2$ with 50% loading at 280 ºC.[130] The interfacial adhesion between carbon sphere and $LiBH_4$-$Mg(BH_4)_2$ was believed to be a critical factor for suppressing agglomeration during dehydrogenation cycles (**Figure 10**). Nanoconfinement altered reaction pathways of eutectic $LiBH_4$–$Mg(BH_4)_2$ as the multistep thermal decomposition pattern became a two-step reaction.[131]

4.3.3 Synergy of Nanostructuring and Catalyst Doping

The synergetic effects of nanostructuring and nanocatalysis have been pursued to further improve hydrogen storage properties of $LiBH_4$ by fabricating catalyst-containing nanostructures. These are summarized in **Table 6**. In 2010, Ngene *et al*. combined nanosized Ni catalyst with nanoporous carbon scaffold-confined $LiBH_4$,[132] and obtained 10 wt% of hydrogen uptake per $LiBH_4$ at 320 ºC under 40 bar H_2 while the Ni-free sample absorbed only 6 wt% H. The presence of Ni significantly enhanced the hydrogen uptake under mild conditions due to the *in situ* formation of Ni_xB.[133] By doping with TiO_2, the dehydrogenation kinetics and reversibility of nanoconfined $LiBH_4$ in activated carbon nanofibers were further improved.[134] In particular, Xian *et al*. constructed an active porous core-shell network with carbon nanotube as the core and nano-TiO_2 decorated porous amorphous carbon as the shell.[135] The hybrid scaffold facilitated high loading of $LiBH_4$ and therefore high catalytic activity. There were reactions between TiO_2 and $LiBH_4$ generating $LiTiO_2$ and TiB_2. At a $LiBH_4$ loading of 60 wt%, the system released 7.3 wt% H within 60 min at 320 ºC, and a reversible capacity of 5.1 wt% was achieved even after 20 cycles. $LiBH_4$ nanoparticles confined by poly(methylmethacrylate) (PMMA) and reduced graphene oxide modified melamine foam (GMF) desorbed 2.9 wt% H within 25 min at 250 ºC, superior to the PMMA-free $LiBH_4$/GMF sample.[136] With nanoconfinement by carbon aerogels and catalysis of CoNiB nanoparticles, $LiBH_4$ released 9.33 wt% H in 30 min at 350 ºC and the activation energy was reduced from 59 kJ mol^{-1} (per

$LiBH_4$) to 46 kJ mol^{-1}.[137] The maximum hydrogen release rate of activated carbon confined $LiBH_4$ doped with CeF_3 as the catalyst was 288 times higher than that of pure $LiBH_4$ at 350 °C.[138] After introducing Ni and Co nanoparticles into N-doped graphene-rich aerogel confined $LiBH_4$, the liberation of hydrogen started at lower temperatures.[139] Very recenlty, Zhang *et al*. achieved reversible desorption and absorption of ~9.2 wt% hydrogen at 300 ºC and under 100 bar H_2 by synthesizing a Ni-decorated graphene-supported $LiBH_4$ nanocomposite ($LiBH_4$ nanoparticles: 5-10 nm, Ni nanocrystals: 2-4 nm).[140] The presence of ultrafine Ni nanocrystals prevented effectively the formation of stable $B_{12}H_{12}^{2-}$ cluster during hydrogen cycling. After 100 cycles, the hydrogen capacity was around 8.5 wt%, corresponding to 92.4% of capacity retention, representing a stable cyclability (**Figure 11**). This is an important breakthrough in long-term cycling of metal borohydrides under mild conditions. Such a remarkable improvement was mainly attributed to the successful suppression of B_2H_6 by-product evolution and the good physical contact between LiH and B after dehydrogenation due to a synergistic effect of nanostructuring and nanocatalysis. Several metal chlorides such as $TiCl_3$, $TiCl_4$ and $ZrCl_4$, were also introduced to nanoconfined $LiBH_4$-MgH_2 systems to achieve the synergistic effect of nanostructuring and nanocatalysis.[141] Faster dehydrogenation kinetics was obtained for these samples. The $TiCl_3$-doped nanoconfined $2LiBH_4$-MgH_2 required only 1 h to release 95% of hydrogen while 2.5 h was needed for the sample without $TiCl_3$. The addition of $TiCl_4$ further reduced the onset dehydrogenation temperature of nanoconfined $2LiBH_4$-MgH_2 by 140 ºC. The formation of Ti–MgH_2 alloy upon the first hydrogenation was believed to be the critical reason. We therefore believe that catalyst-nanoconfinement synergy should be further explored to enable metal borohydrides for practical reversible hydrogen storage applications.

5. Summary and Outlook

Limitations in the use of $LiBH_4$ for hydrogen storage are high opeartion temperatures, slow kinetics and poor reversibility. To address these issues, thermodynamics and kinetics tailoring are essential and considerable work has been conducted, including cation/anion substitution, catalyst doping, reactive compositing and nanoengineering. Partial substitution of cations or anions and compositing with metal and metal hydrides have been widely adopted for thermodynamics tailoring. A variety of bimetallic borohydrides and reactive composites have been developed for this purpose. A representative example is the $2LiBH_4$-MgH_2 system, in which the desorption enthalpy change was reduced by 25 kJ mol^{-1} H_2.

Introducing catalytic additives effectively reduced the operating temperatures for hydrogen storage in $LiBH_4$ by decreasing the kinetic barriers. Carbon materials, metals, metal halides, metal oxides and metal borides have been evaluated and compared. Mechanistic studies revealed that most of metal compounds were converted to borides after first dehydrogenation and hydrogenation. Experimental work highlighted the effectiveness of transition metals and their borides, especially metallic Ni. However, the amount of catalytic additives was often higher than 10 wt%, even up to 50 wt%, which largely reduced the usable hydrogen capacity. Nanoengineering has proved effective in tailoring hydrogen storage kinetics of $LiBH_4$, even to change thermodynamics when the particle size is small enough. Using porous host materials, the operating temperatures for hydrogen storage in $LiBH_4$ have been largely reduced and the hydrogen storage reversibility was significantly improved. However, the inertness of host materials to hydrogen and low loading efficiency need to be addressed. The evolution of B_2H_6 by-product can be effectively prevented by creating reactive composites, doping catalysts and nanoengineering. More importantly, the synergistic effects of nanostructuring and nanocatalysis enabled reversible storage of more than 9 wt% hydrogen with a stable cyclability at much milder conditions (300 ºC and 100 bar H_2), representing an important progress in promoting $LiBH_4$-based hydrogen storage materials for practical mobile applications.

In our eyes, future research should concentrate on the dual tailoring of theremodynamics and kinetics for hydrogen storage in $LiBH_4$-based materials with high capacity, including but not limited to: i) searching for more effective destabilizing agents and fabricating nanosized reactive composite systems; ii) understanding the size-dependent catalytic activity of transition metals and their borides and optimizing their doping approaches; iii) designing and developing synthesis of novel support-free nanostructures of $LiBH_4$; iv) developing *in-situ* simultaneous formation of nanostructured $LiBH_4$ and nanocatalysts without supports; and v) understanding the underlying mechanisms of nanosynergy between nanostructuring and nanocatalysis for $LiBH_4$-based hydrogen storage systems. With these efforts, we hope to see further development in high-capacity $LiBH_4$-based hydrogen storage materials with favorable theremodyamics and kinetics in the near future.

Acknowledgements

W. Z. and X. Z. contributed equally to this work. This work was supported by the National Key R&D Program of China (2018YFB1502102), the Natural Science Foundation of Zhejiang Province (LD21E010002), the National Natural Science Foundation of China (52001277, 52071287), and the National Youth Top-Notch Talent Support Program. Z.H. acknowledges support under the Australian Research Council's (ARC) Discovery Projects funding scheme (DP170101773) and an ARC Future Fellowship (FT190100658).

Received: ((will be filled in by the editorial staff))
Revised: ((will be filled in by the editorial staff))
Published online: ((will be filled in by the editorial staff))

References

[1] a) M. S. Dresselhaus, I. L. Thomas, *Nature*, 2001, 414, 332; b) S. Chu, A. Majumdar, *Nature*, 2012, 488, 294; c) S. M. Hwang, Y.-G. Lim, J.-G. Kim, Y.-U. Heo, J. H. Lim, Y. Yamauchi, M.-S. Park, Y.-J. Kim, S. X. Dou, J. H. Kim, *Nano Energy*, 2014, 10, 53; d) J. Lee, J. Moon, S. A. Han, J. Kim, V. Malgras, Y.-U. Heo, H. Kim, S.-M. Lee, H. K. Liu, S. X. Dou, Y. Yamauchi, M.-S. Park, J. H. Kim, *ACS Nano*, 2019, 13, 9607; e) H. R. Xue, J. Q. Zhao, J. Tang, H. Gong, P. He, H. S. Zhou, Y. Yamauchi, J. P. He, *Chem. Eur. J.*

2016, 22, 4915; f) S. M. Hwang, S. Y. Kim, J.-G. Kim, K. J. Kim, J.-W. Lee, M.-S. Park, Y.-J. Kim, M. Shahabuddin, Y. Yamauchi, J. H. Kim, *Nanoscale*, 2015, 7, 8351.

[2] a) L. Schlapbach, A. Züttel, *Nature* **2001**, *414*, 353; b) T. He, P. Pachfule, H. Wu, Q. Xu, P. Chen, *Nature Rev. Mater*. **2016**, *1*, 16059.

[3] a) A. Midilli, I. Dincer, *Int. J. Hydrogen Energy*, 2007, 32, 511; b) I. P. Jain, *Int. J. Hydrogen Energy*, 2009, 34, 7368; c) J. O. Abe, A. P. I. Popoola, E. Ajenifuja, O. M. Popoola, Int. *J. Hydrogen Energy*, 2019, 44, 15072.

[4] H. Yumiya, M. Kizaki, H. Asai, *World Electr. Veh. J.* **2015**, *7*, 85.

[5] a) M. Momirlan, T. N. Veziroglu, *Renew. Sustain. Energy Rev.*, 2002, 6, 141; b) E. I. Zoulias, N. Lymberopoulos, Hydrogen-based Autonomous Power Systems, Springer, London, 2008; c) Z. X. Liu, Z. M. Qiu, Y. Luo, Z. Q. Mao, C. Wang, *Int. J. Hydrogen Energy*, 2010, 35, 2762; d) F. Sorgulu, I. Dincer, *Int. J. Hydrogen Energy*, 2018, 43, 5842.

[6] a) L. Schlapbach, *Nature* **2009**, *460*, 809; b) K. T. Møller, T. R. Jensen, E. Akiba, H. W. Li, *Prog. Nat. Sci.: Mater. Int*. **2017**, *27*, 34; c) Q. L. Zhu, Q. Xu, *Energy Environ. Sci.* **2015**, *8*, 478; d) R. Mohtadi, S. Orimo, *Nat. Rev. Mater.* **2016**, *2*, 16091.

[7] a) U. Eberle, M. Felderhoff, F. Schüth, *Angew. Chem. Int. Ed.* **2009**, *48*, 6608; b) D. J. Durbin, C. Malardier-Jugroot, *Int. J. Hydrogen Energy* **2013**, *38*, 14595.

[8] a) V. Bérubé, G. Radtke, M. Dresselhaus, G. Chen, *Int. J. Energy Res.* **2007**, *31*, 637; b) P. Chen, M. Zhu, *Mater. Today* **2008**, *11*, 36; c) M. Hirscher, V. A. Yartys, M. Baricco, J. Bellosta von Colbe, D. Blanchard, R. C. Bowman, D. P. Broom, C. E. Buckley, F. Chang, P. Chen, Y. W. Cho, J.-C. Crivello, F. Cuevas, W. I. F. David, P. E. de Jongh, R. V. Denys, M. Dornheim, M. Felderhoff, Y. Filinchuk, G. E. Froudakis, D. M. Grant, E. M. Gray, B. C. Hauback, T. He, T. D. Humphries, T. R. Jensen, S. Kim, Y. Kojima, M. Latroche, H.-W. Li, M. V. Lototskyy, J. W. Makepeace, K. T. Møller, L. Naheed, P. Ngene, D. Noréus, M. M. Nygård, S.-i. Orimo, M. Paskevicius, L. Pasquini, D. B. Ravnsbæk, M. Veronica Sofianos, T. J. Udovic, T. Vegge, G. S. Walker, C. J. Webb, C.

Weidenthaler, C. Zlotea, *J. Alloys Compd.* **2020**, *827*, 153548; d) V. A. Yartys, M. V. Lototskyy, E. Akiba, R. Albert, V. E. Antonov, J. R. Ares, M. Baricco, N. Bourgeois, C. E. Buckley, J. M. Bellosta von Colbe, J. C. Crivello, F. Cuevas, R. V. Denys, M. Dornheim, M. Felderhoff, D. M. Grant, B. C. Hauback, T. D. Humphries, I. Jacob, T. R. Jensen, P. E. de Jongh, J. M. Joubert, M. A. Kuzovnikov, M. Latroche, M. Paskevicius, L. Pasquini, L. Popilevsky, V. M. Skripnyuk, E. Rabkin, M. V. Sofianos, A. Stuart, G. Walker, H. Wang, C. J. Webb, M. Zhu, *Int. J. Hydrogen Energy* **2019**, *44*, 7809; e) X. B. Yu, Z. W. Tang, D. L. Sun, L. Z. Ouyang, M. Zhu, *Prog. Mater. Sci.* **2017**, *88*, 1; f) A. Schneemann, J. L. White, S. Y. Kang, S. Jeong, L. F. Wan, E. S. Cho, T. W. Heo, D. Prendergast, J. J. Urban, B. C. Wood, M. D. Allendorf, V. Stavila, *Chem. Rev.* **2018**, *118*, 10775; g) Q. W. Lai, M. Paskevicius, D. A. Sheppard, C. E. Buckley, A. W. Thornton, M. R. Hill, Q. F. Gu, J. F. Mao, Z. G. Huang, H. K. Liu, Z. P. Guo, A. Banerjee, S. Chakraborty, R. Ahuja, K. F. Aguey-Zinsou, *ChemSusChem* **2015**, *8*, 2789; h) X. Zhang, Y. F. Liu, Z. H. Ren, X. L. Zhang, J. J. Hu, Z. G. Huang, Y. H. Lu, M. X. Gao, H. G. Pan, *Energy Environ. Sci.* **2021**, DOI: 10.1039/D0EE03160G.

[9] a) B. Sakintuna, F. Lamari-Darkrim, M. Hirscher, *Int. J. Hydrogen Energy* **2007**, *32*, 1121; b) P. Chen, Z. T. Xiong, G. T. Wu, Y. F. Liu, J. Hu, W. F. Luo, *Scr. Mater.* **2007**, *56*, 817; c) Y. F. Liu, H. G. Pan, M. X. Gao, Q. D. Wang, *J. Mater. Chem.* **2011**, *21*, 4743; d) Y. F. Liu, Z. H. Ren, X. Zhang, N. Jian, Y. X. Yang, M. X. Gao, H. G. Pan, *Energy Technol.* **2018**, *6*, 487; e) Y. F. Liu, Y. X. Yang, M. X. Gao, H. G. Pan, *Chem. Rec.* **2016**, *16*, 189; f) Y. H. Sun, C. Q. Shen, Q. W. Lai, W. Liu, D. W. Wang, K. F. Aguey-Zinsou, *Energy Storage Mater.* **2018**, *10*, 168; g) R. Kumar, A. Karkamkar, M. Bowden, T. Autrey, *Chem. Soc. Rev.* **2019**, *48*, 5350; h) S. Orimo, Y. Nakamori, J. R. Eliseo, A. Züttel, C. M. Jensen, *Chem. Rev.* **2007**, *107*, 4111; i) J. W. Ren, H. W. Langmi, B. C. North, M. Mathe, *Int. J. Energy Res.* **2015**, *39*, 607; j) A. Salehabadi, M. F. Umar, A. Ahmad, M. I. Ahmad, N. Ismail, M. Rafatullah, *Int. J. Energy Res.* **2020**, *44*, 11044; k) Y. S. Chua, P.

Chen, G. T. Wu, Z. T. Xiong, *Chem. Commun.* **2011**, *47*, 5116.

[10] a) T. He, H. J Cao, P. Chen, *Adv. Mater.* **2019**, *31*, 1902757; b) L. Z. Ouyang, K. Chen, J. Jiang, X. S. Yang, M. Zhu, *J. Alloys Compd.* **2020**, *829*, 154597.

[11] I. P. Jain, P. Jain, A. Jain, *J. Alloys Compd.* **2010**, *503*, 303.

[12] DOE Technical Targets for Onboard Hydrogen Storage for Light-Duty Vehicles, https://www.energy.gov/eere/fuelcells/doe-technical-targets-onboard-hydrogen-storage-light-duty-vehicles, accessed: 2017.

[13] G. L. Soloveichik, *Mater. Matters* **2007**, *2*, 11.

[14] *CRC Handbook of Chemistry and Physics*, CRC Press/Taylor & Francis.

[15] H. Hagemann, R. Černý, *Dalton Trans.* **2010**, *39*, 6006.

[16] a) Y. Filinchuk, D. Chernyshov, V. Dmitriev, *Z. Kristallogr.* **2008**, *223*, 649; b) C. Li, P. Peng, D. W. Zhou, L. Wan, *Int. J. Hydrogen Energy* **2011**, *36*, 14512.

[17] J. P. Soulié, G. Renaudin, R. Černý, K. Yvon, *J. Alloys Compd.* **2002**, *346*, 200.

[18] Y. Filinchuk, D. Chernyshov, A. Nevidomskyy, V. Dmitriev, *Angew. Chem. Int. Ed.* **2008**, *47*, 529.

[19] H. I. Schlesinger, H. C. Brown, *J. Am. Chem. Soc.* **1940**, *62*, 3429.

[20] H. I. Schlesinger, H. C. Brown, B. Abraham, A. C. Bond, N. Davidson, A. E. Finholt, J. R. Gilbreath, H. Hoekstra, L. Horvitz, E. K. Hyde, J. J. Katz, J. Knight, R. A. Lad, D. L. Mayfield, L. Rapp, D. M. Ritter, A. M. Schwartz, I. Sheft, L. D. Tuck, A. O. Walker, *J. Am. Chem. Soc.* **1953**, *75*, 186.

[21] a) O. Friedrichs, F. Buchter, A. Borgschulte, A. Remhof, C. N. Zwicky, P. Mauron, M. Bielmann, A. Züttel, *Acta Mater.* **2008**, *56*, 949; b) P. Mauron, F. Buchter, O. Friedrichs, A. Remhof, M. Bielmann, C. N. Zwicky, A. Züttel, *J. Phys. Chem. B* **2008**, *112*, 906; c) O. Friedrichs, A. Borgschulte, S. Kato, F. Buchter, R. Gremaud, A. Remhof, A. Züttel, *Chem. Eur. J.* **2009**, *15*, 5531.

[22] H. C. Brown, Y. M. Choi, S. Narasimhan, *Inorg. Chem.* **1981**, *20*, 4454.

[23] A. Züttel, P. Wenger, S. Rentsch, P. Sudan, P. Mauron, C. Emmenegger, *J. Power Sources* **2003**, *118*, 1.

[24] A. Züttel, S. Rentsch, P. Fischer, P. Wenger, P. Sudan, P. Mauron, C. Emmenegger, *J. Alloys Compd.* **2003**, *356-357*, 515.

[25] E. M. Fedneva, V. L. Alpatova, V. I. Mikheeva, *Russ. J. Inorg. Chem.* **1964**, *9*, 826.

[26] A. Züttel, A. Borgschulte, S. Orimo, *Scr. Mater.* **2007**, *56*, 823.

[27] O. Friedrichs, A. Remhof, S. J. Hwang, A. Züttel, *Chem. Mater.* **2010**, *22*, 3265.

[28] M. P. Pitt, M. Paskevicius, D. H. Brown, D. A. Sheppard, C. E. Buckley, *J. Am. Chem. Soc.* **2013**, *135*, 6930.

[29] S. Orimo, Y. Nakamori, G. Kitahara, K. Miwa, N. Ohba, S. Towata, A. Züttel, *J. Alloys Compd.* **2005**, *404-406*, 427.

[30] H. W. Li, Y. G. Yan, S. Orimo, A. Züttel, C. M. Jensen, *Energies* **2011**, *4*, 185.

[31] a) D. Ravnsbæk, Y. Filinchuk, Y. Cerenius, H. J. Jakobsen, F. Besenbacher, J. Skibsted, T. R. Jensen, *Angew. Chem., Int. Ed.* **2009**, *48*, 6659; b) Z. Z. Fang, X. D. Kang, J. H. Luo, P. Wang, H. W. Li, S. Orimo, *J. Phys. Chem. C* **2010**, 114, 22736; c) E. A. Nickels, M. O. Jones, W. I. F. David, S. R. Johnson, R. L. Lowton, M. Sommariva, P. P. Edwards, *Angew. Chem., Int. Ed.* **2008**, *47*, 2817; d) Z. Z. Fang, X. D. Kang, P. Wang, H. W. Li, S. Orimo, *J. Alloys Compd.* **2010**, *491*, L1; e) M. Au, M. J. Meziani, Y. P. Sun, F. E. Pinkerton, *J. Phys. Chem. C* **2011**, *115*, 20765; f) M. Paskevicius, M. B. Ley, D. A. Sheppard, T. R. Jensen, C. E. Buckley, *Phys. Chem. Chem. Phys.* **2013**, *15*, 19774; g) E. G. Bardají, Z. Zhao-Karger, N. Boucharat, A. Nale, M. J. Van Setten, W. Lohstroh, E. Röhm, M. Catti, M. Fichtner, *J. Phys. Chem. C* **2011**, *115*, 6095.

[32] a) H. W. Li, S. Orimo, Y. Nakamori, K. Miwa, N. Ohba, S. Towata, A. Züttel, *J. Alloys Compd.* **2007**, *446-447*, 315; b) H. Hagemann, M. Longhini, J. W. Kaminski, T. A. Wesolowski, R. Černý, N. Penin, M. H. Sørby, B. C. Hauback, G. Severa, C. M. Jensen, *J. Phys. Chem. A* **2008**, *112*, 7551.

[33] E. Roedern, B. R. S. Hansen, M. B. Ley, T. R. Jensen, *J. Phys. Chem. C* **2015**, *119*, 25818.

[34] J. Y. Lee, D. Ravnsbæk, Y. S. Lee, Y. Kim, Y. Cerenius, J. H. Shim, T. R. Jensen, N. H. Hur, Y. W. Cho, *J. Phys. Chem. C* **2009**, *113*, 15080.

[35] L. C. Yin, P. Wang, Z. Z. Fang, H. M. Cheng, *Chem. Phys. Lett.* **2008**, *450*, 318.

[36] B. Richter, D. B. Ravnsbæk, M. Sharma, A. Spyratou, H. Hagemann, T. R. Jensen, *Phys. Chem. Chem. Phys.* **2017**, *19*, 30157.

[37] Z. Z. Fang, X. D. Kang, Z. X. Yang, G. S. Walker, P. Wang, *J. Phys. Chem. C* **2011**, *115*, 11839.

[38] L. H. Rude, O. Zavorotynska, L. M. Arnbjerg, D. B. Ravnsbæk, R. A. Malmkjær, H. Grove, B. C. Hauback, M. Baricco, Y. Filinchuk, F. Besenbacher, T. R. Jensen, *Int. J. Hydrogen Energy* **2011**, *36*, 15664.

[39] J. H. Luo, H. Wu, W. Zhou, X. D. Kang, Z. Z. Fang, P. Wang, *Int. J. Hydrogen Energy* **2012**, *37*, 10750.

[40] J. J. Vajo, G. L. Olson, *Scr. Mater.* **2007**, *56*, 829.

[41] J. J. Vajo, S. L. Skeith, F. Mertens, *J. Phys. Chem. B* **2005**, *109*, 3719.

[42] F. E. Pinkerton, M. S. Meyer, G. P. Meisner, M. P. Balogh, J. J. Vajo, *J. Phys. Chem. C* **2007**, *111*, 12881.

[43] a) S. V. Alapati, J. Karl Johnson, D. S. Sholl, *Phys. Chem. Chem. Phys.* **2007**, *9*, 1438; b) J. Yang, A. Sudik, C. Wolverton, *J. Phys. Chem. C* **2007**, *111*, 19134; c) D. J. Siegel, C. Wolverton, V. Ozoliņš, *Phys. Rev. B* **2007**, *76*, 134102; d) X. D. Kang, P, Wang, L. P. Ma, H. M. Cheng, *Appl. Phys. A* **2007**, *89*, 963; e) Q. He, D. D. Zhu, X. C. Wu, D. Dong, M. Xu, Z. F. Tong, *Molecules* **2019**, *24*, 1861; f) F. E. Pinkerton, M. S. Meyer, *J. Alloys Compd.* **2008**, *464*, L1; g) Y. W. Zhang, X. Z. Xiao, B. S. Luo, X. Huang, M. J. Liu, L. X. Chen, *J. Phys. Chem. C* **2018**, *122*, 2528; h) M. R. Ghaani, M. Catti, A. Nale, *J. Phys. Chem. C* **2012**, *116*, 26694; i) Y. P. Pang, Y. F. Liu, X. Zhang, Q. Li, M. X. Gao, H. G. Pan, *Chem. Asian J.* **2015**, *10*, 2452; j) J. J. Vajo, T. T. Salguero, A. F. Gross, S. L. Skeith, G. L. Olson,

J. Alloys Compd. **2007**, *446-447*, 409; k) J. Purewal, S. J. Hwang, J. R. C. Bowman, E. Rönnebro, B. Fultz, C. Ahn, *J. Phys. Chem. C* **2008**, *112*, 8481; l) S. A. Jin, Y. S. Lee, J. H. Shim, Y. W. Cho, *J. Phys. Chem. C* **2008**, *112*, 9520; m) O. Friedrichs, J. W. Kim, A. Remhof, F. Buchter, A. Borgschulte, D. Wallacher, Y. W. Cho, M. Fichtner, K. H. Oh, A. Züttel, *Phys. Chem. Chem. Phys.* **2009**, *11*, 1515; n) Y. Zhang, Q. F. Tian, J. Zhang, S. S. Liu, L. X. Sun, *J. Phys. Chem. C* **2009**, *113*, 18424; o) F. C. Gennari, *Int. J. Hydrogen Energy* **2011**, *36*, 15231; p) Y. F. Zhou, Y. F. Liu, W. Wu, Y. Zhang, M. X. Gao, H. G. Pan, *J. Phys. Chem. C* **2012**, *116*, 1588; q) X. C. Wu, X. H. Wang, G. Z. Cao, S. Q. Li, H. W. Ge, L. X. Chen, M. Yan, *J. Alloys Compd.* **2012**, *517*, 127; r) D. M. Liu, C. Gao, Z. X. Qian, T. Z. Si, Q. A. Zhang, *Int. J. Hydrogen Energy* **2013**, *38*, 3291.

[44] Y. F. Zhou, Y. F. Liu, Y. Zhang, M. X. Gao, H. G. Pan, *Dalton Trans.* **2012**, *41*, 10980.

[45] J. J. Vajo, W. Li, P. Liu, *Chem. Commun.* **2010**, *46*, 6687.

[46] N. Bergemann, C. Pistidda, M. Uptmoor, C. Milanese, A. Santoru, T. Emmler, J. Puszkiel, M. Dornheim, T. Klassen, *J. Energy Chem.* **2019**, *34*, 240.

[47] M. X. Gao, J. Gu, H. G. Pan, Y. L. Wang, Y. F. Liu, C. Liang, Z. X. Guo, *J. Mater. Chem. A* **2013**, *1*, 12285.

[48] E. M. Dematteis, C. Pistidda, M. Dornheim, M. Baricco, *ChemPhysChem* **2019**, *20*, 1348.

[49] M. Ismail, Int. J. Hydrogen Energy, 2014, 39, 8340.

[50] a) F. A. Halim Yap, N. S. Mustafa, M. S. Yahya, A. A. Mohamad, M. Ismail, Int. J. Hydrogen Energy, 2018, 43, 8365; b) F. A. Halim Yap, N. A. Ali, N. H. Idris, M. Ismail, Int. J. Hydrogen Energy, 2018, 43, 20882; c) F. A. Halim Yap, M. Ismail, J. Phys. Chem. C 2018, 122, 23959.

[51] P. Kumari, P. Pal, K. Shinzato, K. Awasthi, T. Ichikawa, A. Jain, M. Kumar, *Int. J. Hydrogen Energy* **2020**, *45*, 16992.

[52] a) F. E. Pinkerton, G. P. Meisner, M. S. Meyer, M. P. Balogh, M. D. Kundrat, *J. Phys. Chem. B* **2005**, *109*, 6; b) M. Aoki, K. Miwa, T. Noritake, G. Kitahara, Y. Nakamori, S.

Orimo, S. Towata, *Appl. Phys. A* **2005**, *80*, 1409; c) Y. F. Liu, K. Luo, Y. F. Zhou, M. X. Gao, H. G. Pan, *J. Alloys Compd.* **2009**, *481*, 473.

[53] X. L. Zheng, G. T. Wu, W. Li, Z. T. Xiong, T. He, J. P. Guo, H. Chen, P. Chen, *Energy Environ. Sci.* **2011**, *4*, 3593.

[54] a) G. J. Lewis, J. W. A. Sachtler, J. J. Low, D. A. Lesch, S. A. Faheem, P. M. Dosek, L. M. Knight, L. Halloran, C. M. Jensen, J. Yang, A. Sudik, D. J. Siegel, C. Wolverton, V. Ozolins, S. Zhang, J. Alloys Compd., 2007, 446-447, 355; b) J. R. Hattrick-Simpers,, J. E. Maslar, M. U. Niemann, C. Chiu, S. S. Srinivasan, E. K. Stefanakos, L. A. Bendersky, Int. J. Hydrogen Energy, 2010, 35, 6323; c) A. Sudik, J. Yang, D. Halliday, C. Wolverton, J. Phys. Chem. C, 2008, 112, 4384.

[55] a) X. B. Yu, D. M. Grant, G. S. Walker, *J. Phys. Chem. C* **2009**, *113*, 17945; b) M. Au, A. R. Jurgensen, W. A. Spencer, D. L. Anton, F. E. Pinkerton, S. J. Hwang, C. Kim, R. C. Bowman, *J. Phys. Chem. C* **2008**, *112*, 18661; c) B. J. Zhang, B. H. Liu, *Int. J. Hydrogen Energy* **2010**, *35*, 7288l d) B. J. Zhang, B. H. Liu, Z. P. Li, *J. Alloys Compd.* **2011**, *509*, 751; e) G. L. Xia, Y. H. Guo, Z. Wu, X. B. Yu, *J. Alloys Compd.* **2009**, *479*, 545.

[56] Y. F. Liu, H. A. I. Zhou, Y. F. Ding, M. X. Gao, H. G. Pan, *Funct. Mater. Lett.* **2011**, *04*, 395.

[57] J. Xu, Y. Li, J. Y. Cao, R. R. Meng, W. C. Wang, Z. D. Chen, *Catal. Sci. Technol.* **2015**, *5*, 1821.

[58] X. H. Meng, C. B. Wan, Y. T. Wang, X. Ju, *J. Alloys Compd.* **2018**, *735*, 1637.

[59] a) Z. N. Huang, Y. Q. Wang, D. Wang, F. S. Yang, Z. Wu, Z. X. Zhang, *Comput. Theor. Chem.* **2018**, *1133*, 33; b) X. H. Mo, W. Q. Jiang, S. L. Cao, *Results Phys.* **2017**, *7*, 3236.

[60] a) Y. P. Fan, D. D. Chen, X. Y. Liu, G. X. Fan, B. Z. Liu, *Int. J. Hydrogen Energy* **2019**, *44*, 29297; b) J. S. Wang, Z. B. Wang, Y. Li, D. D. Ke, X. Z. Lin, S. M. Han, M. Z. Ma, *Int. J. Hydrogen Energy* **2016**, *41*, 13156; c) J. Zhang, P. Li, Q. Wan, F. Q. Zhai, A. A.

Volinsky, X. H. Qu, *RSC Adv.* **2015**, *5*, 81212.

[61] Z. Z. Fang, X. D. Kang, H. B. Dai, M. J. Zhang, P. Wang, H. M. Cheng, *Scr. Mater.* **2008**, *58*, 922.

[62] Z. Z. Fang, X. D. Kang, P. Wang, *Int. J. Hydrogen Energy* **2010**, *35*, 8247.

[63] F. Agresti, A. Khandelwal, G. Capurso, S. L. Russo, A. Maddalena, G. Principi, *Nanotechnology* **2010**, *21*, 065707.

[64] R. H. Scheicher, S. Li, C. M. Araujo, A. Blomqvist, R. Ahuja, P. Jena, *Nanotechnology* **2011**, *22*, 335401.

[65] J. Xu, R. R. Meng, J. Y. Cao, X. F. Gu, Z. Q. Qi, W. C. Wang, Z. D. Chen, *Int. J. Hydrogen Energy* **2013**, *38*, 2796.

[66] W. Zhang, G. Xu, L. J. Chen, S. Y. Pan, X. Jing, J. S. Wang, S. M. Han, *Int. J. Hydrogen Energy* **2017**, *42*, 15262.

[67] X. D. Zhao, Z. N. Ma, D. H. Wu, X. Zhang, Y. Jing, Z. Zhou, *Int. J. Hydrogen Energy* **2015**, *40*, 8897.

[68] X. Huang, X. Z. Xiao, X. C. Wang, Z. D. Yao, C. T. Wang, X. L. Fan, L. X. Chen, *Energy Storage Mater.* **2018**, *13*, 199.

[69] Y. F. Ma, Y. Li, T. Liu, X. Zhao, L. Zhang, S. M. Han, Y. J. Wang, *J. Alloys Compd.* **2016**, *689*, 187.

[70] Z. L. Li, M. X. Gao, J. Gu, K. C. Xian, Z. H. Yao, C. X. Shang, Y. F. Liu, Z. X. Guo, H. G. Pan, *ACS Appl. Mater. Interfaces* **2020**, *12*, 893.

[71] P. E. de Jongh, P. Adelhelm, *ChemSusChem* **2010**, *3*, 1332.

[72] a) Y. P. Pang, Y. F. Liu, M. X. Gao, L. Z. Ouyang, J. W. Liu, H. Wang, M. Zhu, H. G. Pan, *Nat. Commun.* **2014**, *5*, 3519; b) Y. T. Li, Q. G. Zhang, F. Fang, Y. Song, D. Sun, L. Z. Ouyang, M. Zhu, *RSC Adv.* **2014**, *4*, 983; c) T. Wang, K. F. Aguey-Zinsou, *Energy Technol.* **2019**, *7*, 1801159; d) L. Wang, M. Z. Quadir, K. F. Aguey-Zinsou, *Int. J. Hydrogen Energy* **2016**, *41*, 6376; e) Q. W. Lai, T. Wang, Y. H. Sun, K. F. Aguey-Zinsou,

Adv. Mater. Technol. **2018**, *3*, 1700298.

[73] A. F. Gross, J. J. Vajo, S. L. Van Atta, G. L. Olson, *J. Phys. Chem. C* **2008**, *112*, 5651.

[74] S. Cahen, J. B. Eymery, R. Janot, J. M. Tarascon, *J. Power Sources* **2009**, *189*, 902.

[75] M. Christian, K. F. Aguey-Zinsou, *Nanoscale* **2010**, *2*, 2587.

[76] X. F. Liu, D. Peaslee, C. Z. Jost, E. H. Majzoub, *J. Phys. Chem. C* **2010**, 114, 14036.

[77] X. Liu, D. Peaslee, C. Z. Jost, T. F. Baumann, E. H. Majzoub, *Chem. Mater.* **2011**, *23*, 1331.

[78] S. Thiangviriya, R. Utke, *Int. J. Hydrogen Energy* **2015**, *40*, 4167.

[79] R. Gosalawit-Utke, S. Meethom, C. Pistidda, C. Milanese, D. Laipple, T. Saisopa, A. Marini, T. Klassen, M. Dornheim, *Int. J. Hydrogen Energy* **2014**, *39*, 5019.

[80] S. Wang, M. X. Gao, K. C. Xian, Z. L. Li, Y. Shen, Z. H. Yao, Y. F. Liu, H. G. Pan, *ACS Appl. Energy Mater.* **2020**, *3*, 3928.

[81] W. W. Sun, S. F. Li, J. F. Mao, Z. P. Guo, H. K. Liu, S. X. Dou, X. B. Yu, *Dalton Trans.* **2011**, *40*, 5673.

[82] L. L. Guo, Y. Li, Y. F. Ma, Y. Liu, D. D. Peng, L. Zhang, S. M. Han, *Int. J. Hydrogen Energy* **2017**, *42*, 2215.

[83] J. Shao, X. Z. Xiao, X. L. Fan, X. Huang, B. Zhai, S. Q. Li, H. W. Ge, Q. D. Wang, L. X. Chen, *Nano Energy* **2015**, *15*, 244.

[84] T. Sun, J. Liu, Y. Jia, H. Wang, D. L. Sun, M. Zhu, X. D. Yao, *Int. J. Hydrogen Energy* **2012**, *37*, 18920.

[85] R. Y. Wu, X. Zhang, Y. F. Liu, L. C. Zhang, J. J. Hu, M. X. Gao, H. G. Pan, *Small* **2020**, *16*, 2001963.

[86] a) H. Q. Liu, L. F. Jiao, Y. P. Zhao, K. Z. Cao, Y. C. Liu, Y. J. Wang, H. T. Yuan, *J. Mater. Chem. A* **2014**, *2*, 9244; b) X. Xu, L. Zang, Y. Zhao, Y. Liu, Y. Wang, L. Jiao, *Int. J. Hydrogen Energy* **2017**, 42, 25824; c) X. H. Xu, L. Zang, Y. R. Zhao, Y. Zhao, Y. J. Wang, L. F. Jiao, *J. Power Sources* **2017**, *359*, 134; d) L. Zang, W. Y. Sun, S. Liu, Y. K.

Huang, H. T. Yuan, Z. L. Tao, Y. J. Wang, *ACS Appl. Mater. Interfaces* **2018**, *10*, 19598.

[87] G. L. Xia, Y. B. Tan, X. W. Chen, F. Fang, D. L. Sun, X. G. Li, Z. P. Guo, X. B. Yu, *Adv. Sci.* **2017**, *4*, 1600257.

[88] P. Sridechprasat, Y. Suttisawat, P. Rangsunvigit, B. Kitiyanan, S. Kulprathipanja, *Int. J. Hydrogen Energy* **2011**, *36*, 1200.

[89] J. Shao, X. Z. Xiao, L. X. Chen, X. L. Fan, S. Q. Li, H. W. Ge, Q. D. Wang, *J. Mater. Chem.* **2012**, *22*, 20764.

[90] a) H. Q. Kou, X. Z. Xiao, J. X. Li, S. Q. Li, H. W. Ge, Q. D. Wang, L. X. Chen, *Int. J. Hydrogen Energy* **2012**, *37*, 1021; b) X. Z. Xiao, J. Shao, L. X. Chen, H. Q. Kou, X. L. Fan, S. S. Deng, L. T. Zhang, S. Q. Li, H. W. Ge, Q. D. Wang, *Int. J. Hydrogen Energy* **2012**, *37*, 13147; c) H. Q. Kou, G. Sang, Z. Y. Huang, W. H. Luo, L. X. Chen, X. Z. Xiao, C. W. Hu, Y. L. Zhou, *Int. J. Hydrogen Energy* **2014**, *39*, 7050.

[91] J. F. Mao, Z. P. Guo, X. B. Yu, H. K. Liu, *Int. J. Hydrogen Energy* **2013**, *38*, 3650.

[92] G. L. Xia, H. Y. Leng, N. X. Xu, Z. L. Li, Z. Wu, J. L. Du, X. B. Yu, *Int. J. Hydrogen Energy* **2011**, *36*, 7128.

[93] a) X. D. Kang, K. K. Wang, Y. J. Zhong, B. Yang, P. Wang, *Phys. Chem. Chem. Phys.* **2013**, *15*, 2153; b) F. Karimi, M. V. C. Riglos, A. Santoru, A. Hoell, V. S. Raghuwanshi, C. Milanese, N. Bergemann, C. Pistidda, P. Nolis, M. D. Baro, G. Gizer, T. T. Le, P. K. Pranzas, M. Dornheim, T. Klassen, A. Schreyer, J. Puszkiel, *J. Phys. Chem. C* **2018**, *122*, 11671.

[94] X. L. Fan, X. Z. Xiao, L. X. Chen, X. H. Wang, S. Q. Li, H. W. Ge, Q. D. Wang, *J. Mater. Chem. A* **2013**, *1*, 11368.

[95] Y. P. Zhao, L. Z. Ding, T. S. Zhong, H. T. Yuan, L. F. Jiao, *Int. J. Hydrogen Energy* **2014**, *39*, 11055.

[96] Y. Jiang, B. H. Liu, *J. Alloys Compd.* **2011**, *509*, 9055.

[97] B. C. Weng, X. B. Yu, Z. Wu, Z. L. Li, T. S. Huang, N. X. Xu, J. Ni, *J. Alloys Compd.*

2010, *503*, 345.

[98] J. F. Mao, Z. P. Guo, X. B. Yu, H. K. Liu, *J. Alloys Compd.* **2011**, *509*, 5012.

[99] J. A. Puszkiel, F. C. Gennari, P. A. Larochette, J. M. Ramallo-López, U. Vainio, F. Karimi, P. K. Pranzas, H. Troiani, C. Pistidda, J. Jepsen, M. Tolkiehn, E. Welter, T. Klassen, J. Bellosta von Colbe, M. Dornheim, *J. Power Sources* **2015**, *284*, 606.

[100] H. Y. Shao, M. Felderhoff, C. Weidenthaler, *J. Phys. Chem. C* **2015**, *119*, 2341.

[101] M. Q. Fan, L. X. Sun, Y. Zhang, F. Xu, J. Zhang, H. L. Chu, *Int. J. Hydrogen Energy* **2008**, *33*, 74.

[102] U. Bösenberg, J. W. Kim, D. Gosslar, N. Eigen, T. R. Jensen, J. M. B. von Colbe, Y. Zhou, M. Dahms, D. H. Kim, R. Günther, Y. W. Cho, K. H. Oh, T. Klassen, R. Bormann, M. Dornheim, *Acta Mater.* **2010**, *58*, 3381.

[103] J. A. Puszkiel, M. V. Castro Riglos, F. Karimi, A. Santoru, C. Pistidda, T. Klassen, J. M. Bellosta von Colbe, M. Dornheim, *Phys. Chem. Chem. Phys.* **2017**, *19*, 7455.

[104] H. Zhang, Y. X. Zhou, L. X. Sun, Z. Cao, F. Li, *Chem. J. Chinese U.* **2012**, *33*, 781.

[105] J. S. Wang, S. M. Han, Z. B. Wang, D. D. Ke, J. J. Liu, M. Z. Ma, *Dalton Trans.* **2016**, *45*, 7042.

[106] U. Bösenberg, S. Doppiu, L. Mosegaard, G. Barkhordarian, N. Eigen, A. Borgschulte, T. R. Jensen, Y. Cerenius, O. Gutfleisch, T. Klassen, M. Dornheim, R. Bormann, *Acta Mater.* **2007**, *55*, 3951.

[107] E. Deprez, A. Justo, T. C. Rojas, C. López-Cartés, C. Bonatto Minella, U. Bösenberg, M. Dornheim, R. Bormann, A. Fernández, *Acta Mater.* **2010**, *58*, 5683.

[108] P. J. Wang, Z. Z. Fang, L. P. Ma, X. D. Kang, P. Wang, *Int. J. Hydrogen Energy* **2008**, *33*, 5611.

[109] K. K. Wang, X. D. Kang, J. H. Luo, C. C. Hu, P. Wang, *Int. J. Hydrogen Energy* **2013**, *38*, 3710.

[110] I. H. Cho, S. Gang, H. Lee, J. H. Shim, M. Park, Y. N. Choi, *Int. J. Hydrogen Energy*

2016, *41*, 22090.

[111] F. Cova, F. C. Gennari, P. A. Larochette, *RSC Adv.* **2015**, *5*, 90014.

[112] P. Plerdsranoy, S. Chanthee, R. Utke, *Int. J. Hydrogen Energy* **2017**, *42*, 978.

[113] a) J. Chen, Y. Zhang, Z. T. Xiong, G. T. Wu, H. Chu, T. He, P. Chen, *Int. J. Hydrogen Energy* **2012**, *37*, 12425; b) Y. Zhang, Z. Y. Lan, N. Jian, Z. Ren, J. J. Hu, M. X. Gao, H. G. Pan, Y. H. Lu, Y. F. Liu, *Catal. Sci. Technol.* **2017**, *7*, 1838; c) Y. Zhang, Y. F. Liu, Y. X. Yang, Y. Li, J. J. Hu, M. X. Gao, H. G. Pan, *Mater. Res. Bull.* **2018**, *97*, 544.

[114] T. K. Nielsen, U. Bösenberg, R. Gosalawit, M. Dornheim, Y. Cerenius, F. Besenbacher, T. R. Jensen, *ACS Nano* **2010**, *4*, 3903.

[115] R. Gosalawit-Utke, T. K. Nielsen, I. Saldan, D. Laipple, Y. Cerenius, T. R. Jensen, T. Klassen, M. Dornheim, *J. Phys. Chem. C* **2011**, *115*, 10903.

[116] R. Gosalawit-Utke, C. Milanese, T. K. Nielsen, F. Karimi, I. Saldan, K. Pranzas, T. R. Jensen, A. Marini, T. Klassen, M. Dornheim, *Int. J. Hydrogen Energy* **2013**, *38*, 1932.

[117] R. Gosalawit–Utke, S. Thiangviriya, P. Javadian, D. Laipple, C. Pistidda, N. Bergemann, C. Horstmann, T. R. Jensen, T. Klassen, M. Dornheim, *Int. J. Hydrogen Energy* **2014**, *39*, 15614.

[118] G. L. Xia, Y. B. Tan, F. L. Wu, F. Fang, D. L. Sun, Z. P. Guo, Z. G. Huang, X. B. Yu, *Nano Energy* **2016**, *26*, 488.

[119] a) Z. Ding, Y. Lu, L. Li, L. Shaw, *Energy Storage Mater.* **2019**, *20*, 24; b) Z. Ding, L. Shaw, *ACS Sustainable Chem. Eng.* **2019**, *7*, 15064; c) Z. Ding, H. Li, L. Shaw, *Chem. Eng. J.* **2020**, *385*, 123856.

[120] P. Javadian, C. Zlotea, C. M. Ghimbeu, M. Latroche, T. R. Jensen, *J. Phys. Chem. C* **2015**, *119*, 5819.

[121] P. Plerdsranoy, R. Utke, *Int. J. Hydrogen Energy* **2015**, *40*, 7083.

[122] P. Javadian, D. A. Sheppard, C. E. Buckley, T. R. Jensen, *Crystals* **2016**, *6*, 70

[123] P. Plerdsranoy, R. Utke, *J. Phys. Chem. Solids* **2016**, *90*, 80.

[124] H. S. Lee, Y. S. Lee, J. Y. Suh, M. Kim, J. S. Yu, Y. W. Cho, *J. Phys. Chem. C* **2011**, *115*, 20027.

[125] H. S. Lee, S. J. Hwang, H. K. Kim, Y. S. Lee, J. Park, J. S. Yu, Y. W. Cho, *J. Phys. Chem. Lett.* **2012**, *3*, 2922.

[126] P. Javadian, D. A. Sheppard, C. E. Buckley, T. R. Jensen, *Nano Energy* **2015**, *11*, 96.

[127] P. Javadian, D. A. Sheppard, C. E. Buckley, T. R. Jensen, *Int. J. Hydrogen Energy* **2015**, *40*, 14916.

[128] F. Peru, S. Payandeh, G. Charalambopoulou, T. R. Jensen, T. Steriotis, *C-J. Carbon Res.* **2020**, *6*, 19.

[129] P. Javadian, T. R. Jensen, *Int. J. Hydrogen Energy* **2014**, *39*, 9871.

[130] J. G. Zheng, Z. D. Yao, X. Z. Xiao, X. C. Wang, J. H. He, M. Chen, H. Cheng, L. T. Zhang, L. X. Chen, *Int. J. Hydrogen Energy* **2021**, *46*, 852.

[131] Z. Zhao-Karger, R. Witter, E. G. Bardají, D. Wang, D. Cossement, M. Fichtner, *J. Mater. Chem. A* **2013**, *1*, 3379.

[132] P. Ngene, M. van Zwienen, P. E. de Jongh, *Chem. Commun.* **2010**, *46*, 8201.

[133] P. Ngene, M. H. W. Verkuijlen, Q. Zheng, J. Kragten, P. J. M. van Bentum, J. H. Bitter, P. E. de Jongh, *Faraday Discuss.* **2011**, *151*, 47.

[134] C. Sitthiwet, S. Thiangviriya, N. Thaweelap, S. Meethom, D. Kaewsuwan, N. Chanlek, R. Utke, *J. Phys. Chem. Solids* **2017**, *110*, 344.

[135] K. C. Xian, B. Nie, Z. G. Li, M. X. Gao, Z. L. Li, C. X. Shang, Y. F. Liu, Z. X. Guo, H. G. Pan, *Chem. Eng. J.* **2021**, *407*, 127156.

[136] Y. D. Fan, D. D. Chen, Z. L. Yuan, Q. Chen, G. X. Fan, D. Zhao, B. Z. Liu, *Front. Chem.* **2020**, *8*, 45.

[137] Y. P. Zhao, L. F. Jiao, Y. C. Liu, L. J. Guo, L. Li, H. Q. Liu, Y. J. Wang, H. T. Yuan, *Int. J. Hydrogen Energy* **2014**, *39*, 917.

[138] H. Zhou, L. T. Zhang, S. C. Gao, H. Z. Liu, L. Xu, X. H. Wang, M. Yan, *Int. J. Hydrogen*

Energy **2017**, *42*, 23010.

[139] A. Gasnier, G. Amica, J. Juan, H. Troiani, F. C. Gennari, *J. Phys. Chem. C* **2020**, *124*, 115.

[140] X. Zhang, L. C. Zhang, W. X. Zhang, Z. H. Ren, Z. G. Huang, J. J. Hu, M. X. Gao, H. G. Pan, Y. F. Liu, *Nano Energy* **2021**, *83*, 105839.

[141] a) R. Gosalawit-Utke, C. Milanese, P. Javadian, J. Jepsen, D. Laipple, F. Karmi, J. Puszkiel, T. R. Jensen, A. Marini, T. Klassen, M. Dornheim, *Int. J. Hydrogen Energy* **2013**, *38*, 3275; b) R. Gosalawit-Utke, C. Milanese, P. Javadian, A. Girella, D. Laipple, J. Puszkiel, A. S. Cattaneo, C. Ferrara, J. Wittayakhun, J. Skibsted, T. R. Jensen, A. Marini, T. Klassen, M. Dornheim, *J. Alloys Compd.* **2014**, *599*, 78; c) R. Utke, S. Thiangviriya, P. Javadian, T. R. Jensen, C. Milanese, T. Klassen, M. Dornheim, *Mater. Chem. Phys.* **2016**, *169*, 136.

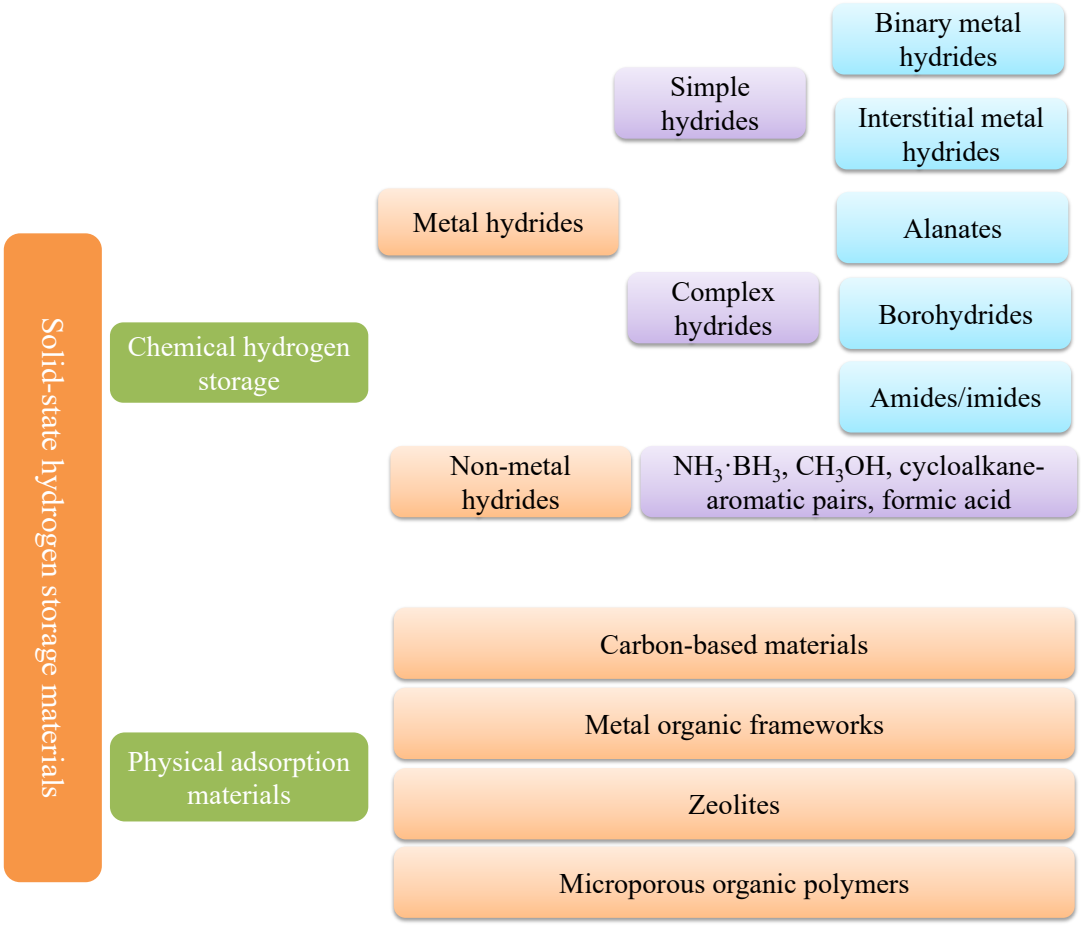

Figure 1 Classification of solid hydrogen storage materials.

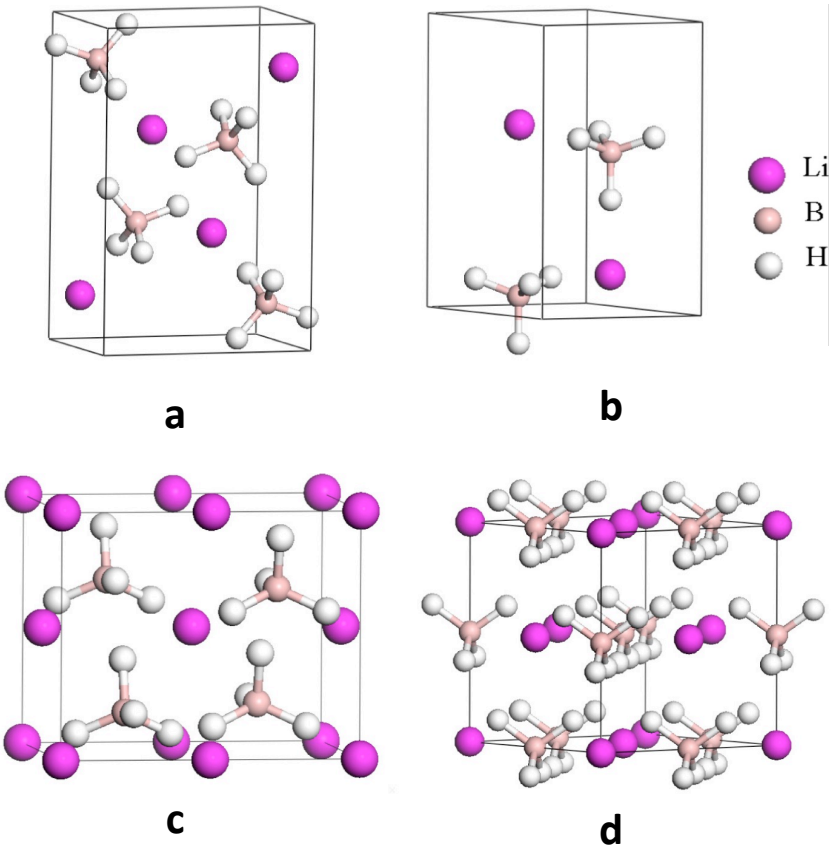

Figure 2 Four crystal structures of $LiBH_4$: (a) Pnma, (b) $P6_3mc$, (c) Ama2, and (d) Fm-3m. Reproduced with permission.[16b] Copyright 2011, Elsevier.

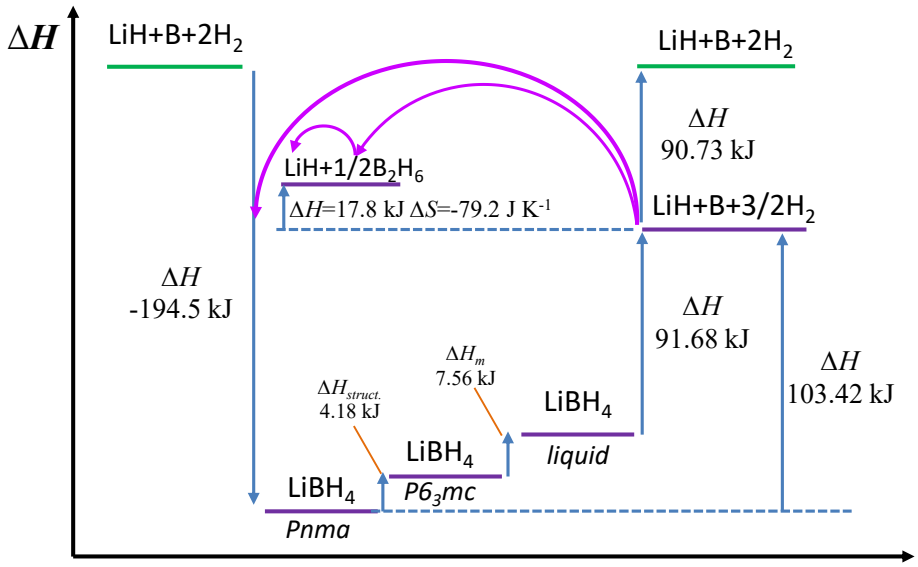

Figure 3 Enthalpy diagram of the phases and intermediate products of $LiBH_4$. Reproduced with permission.[26] Copyright 2007, Elsevier.

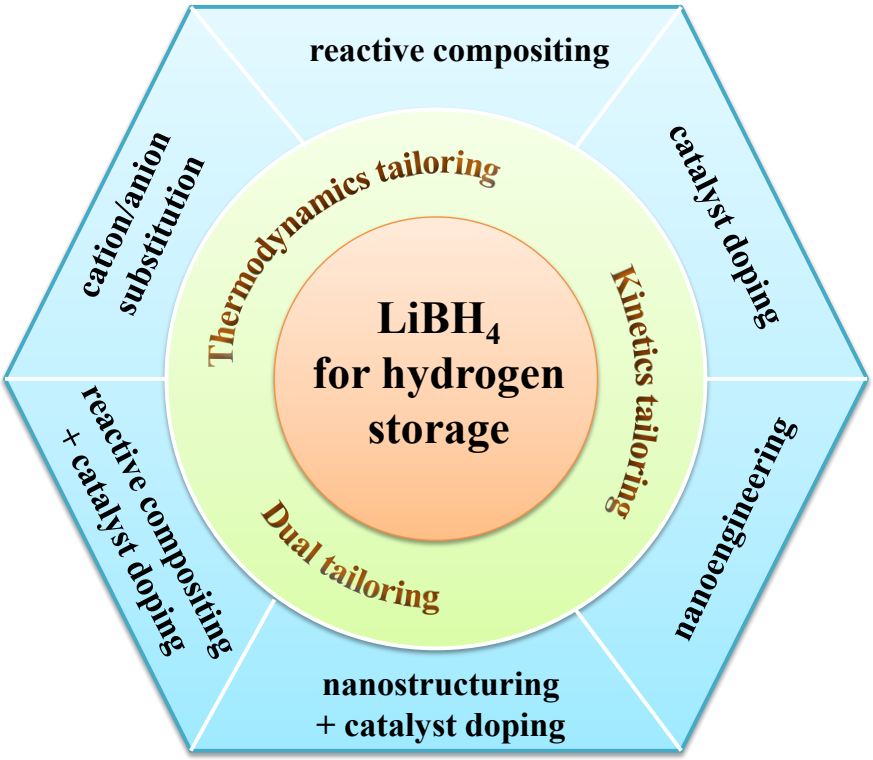

Figure 4 Strategies to tailor thermodynamics and kinetics of hydrogen cycling by $LiBH_4$.

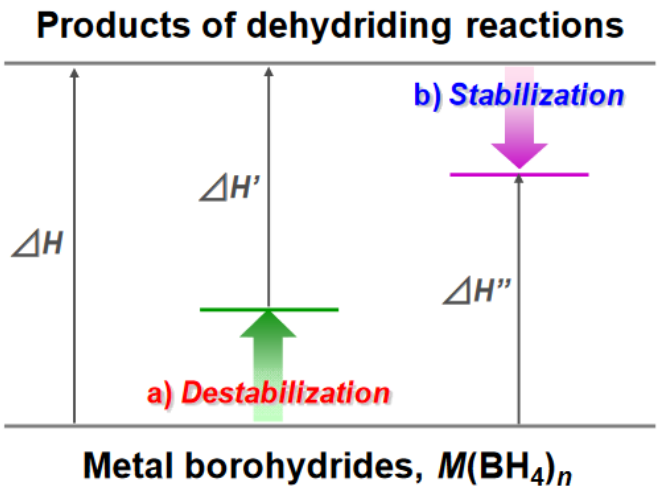

Figure 5 Schematic illustration of two main approaches to tailor the thermodynamic stabilities of metal borohydrides.[30]

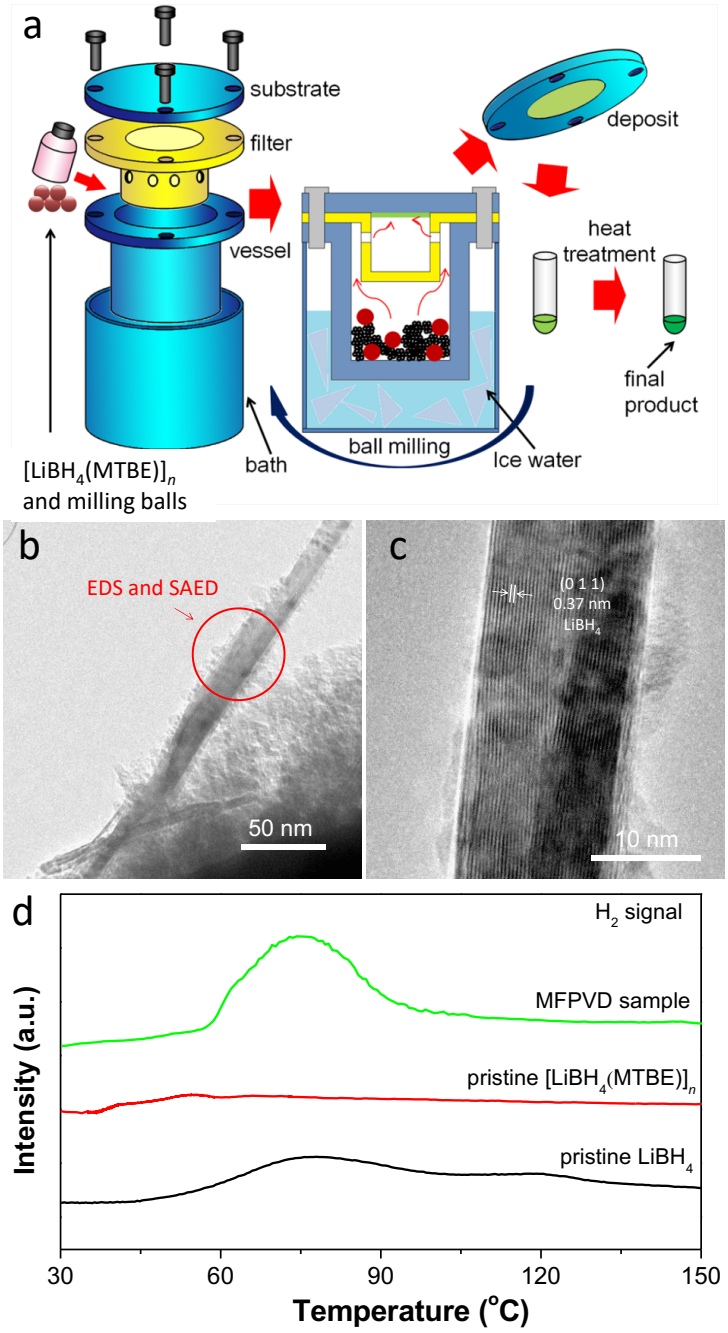

Figure 6 Schematic illustration of (a) the preparation process, (b) TEM image, (c) HRTEM image and (d) TPD-MS of the $LiBH_4$ nanobelts. Reproduced with permission.[72a] Copyright 2014, Springer Nature.

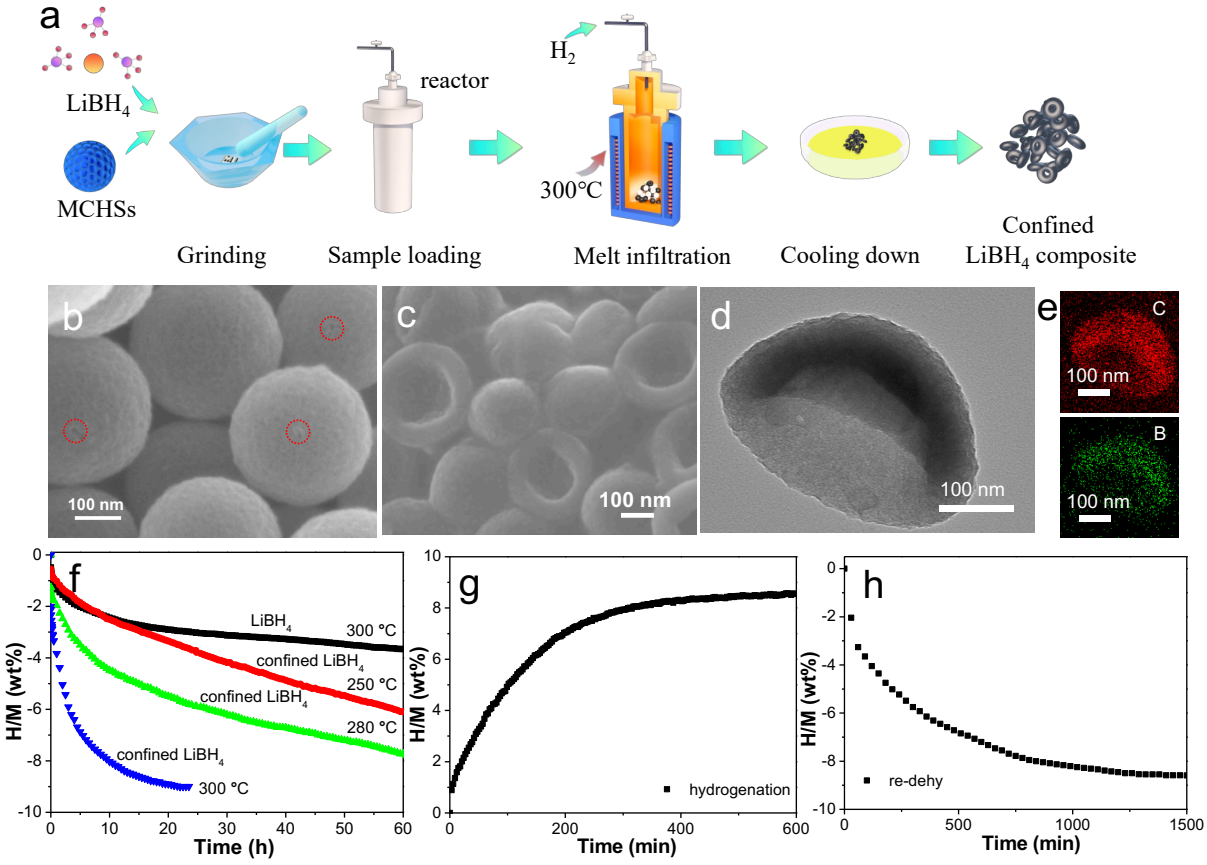

Figure 7 (a) Schematic illustration of the melt infiltration procedure; (b) SEM image of mesoporous carbon hollow spheres (MCHSs); (c) SEM, (d) TEM image, (e) STEM-EDS mapping, (f) hydrogen desorption, (g) absorption (g), and (h) 2nd desorption curves of MCHSs-confined $LiBH_4$ (80 wt% loading). Reproduced with permission.[85] Copyright 2020, Wiley.

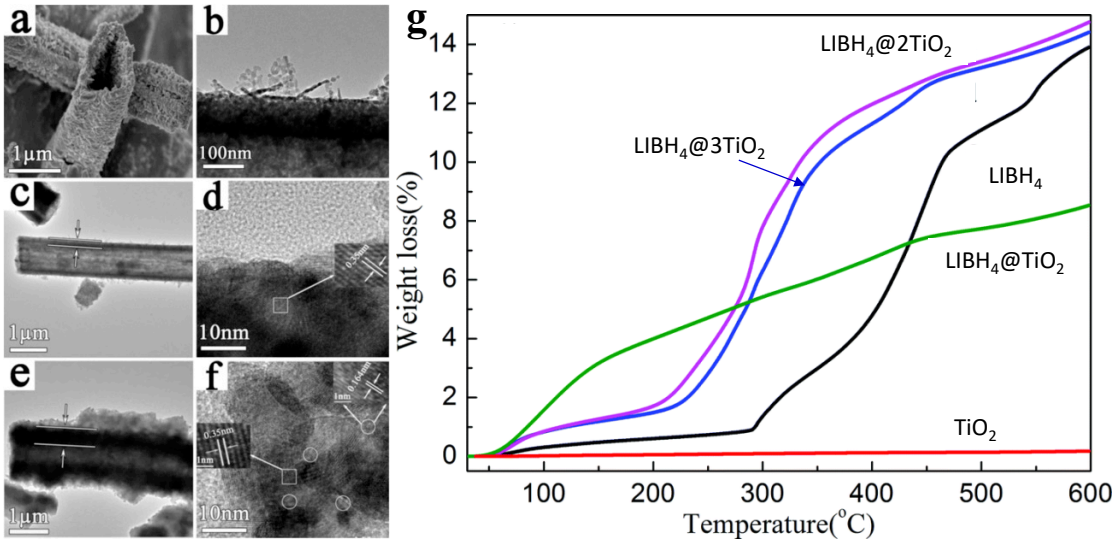

Figure 8 (a) SEM, (b, c) TEM, and (d) HRTEM of the as-prepared TiO_2; (e) TEM, (f) HRTEM and (g) hydrogen desorption curves of $LiBH_4$@TiO_2 composites. Reproduced with permission.[86a] Copyright 2014, RSC Publishing.

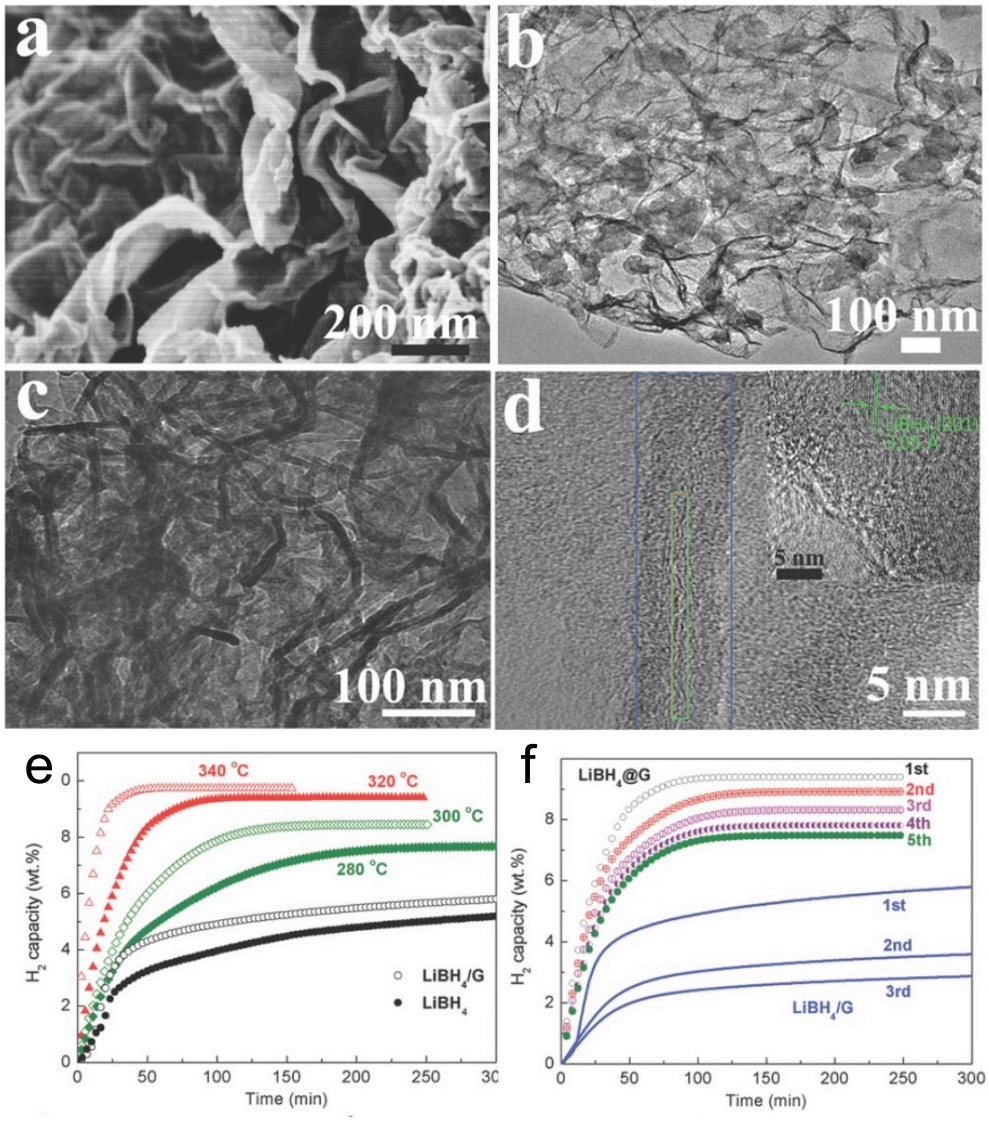

Figure 9 (a) SEM, (b, c) TEM, (d) HRTEM, (e) hydrogen desorption and (f) cycling of the as-synthesized $LiBH_4$@G. Reproduced with permission.[87] Copyright 2017, Wiley.

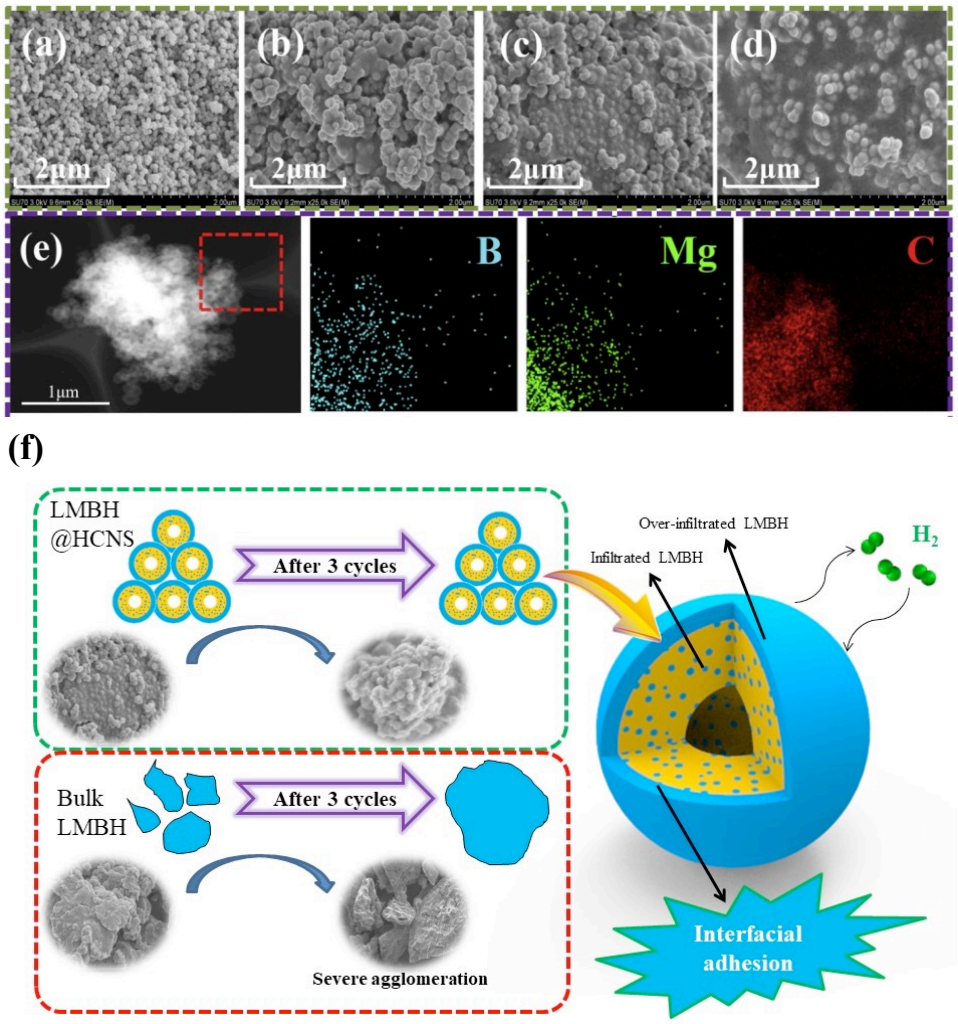

Figure 10 (a) SEM images of hollow carbon nanospheres (HCNS), (b) 30LMBH@HCNS, (c) 50LMBH@HCNS and (d) 67LMBH@HCNS composites, (e) HAADF TEM observation and corresponding EDS mapping of 50LMBH@HCNS composite, and (f) schematic illustration of the improved reversible hydrogen storage properties of over-infiltrated 50LMBH@HCNS composite. Reproduced with permission.[130] Copyright 2021, Elsevier.

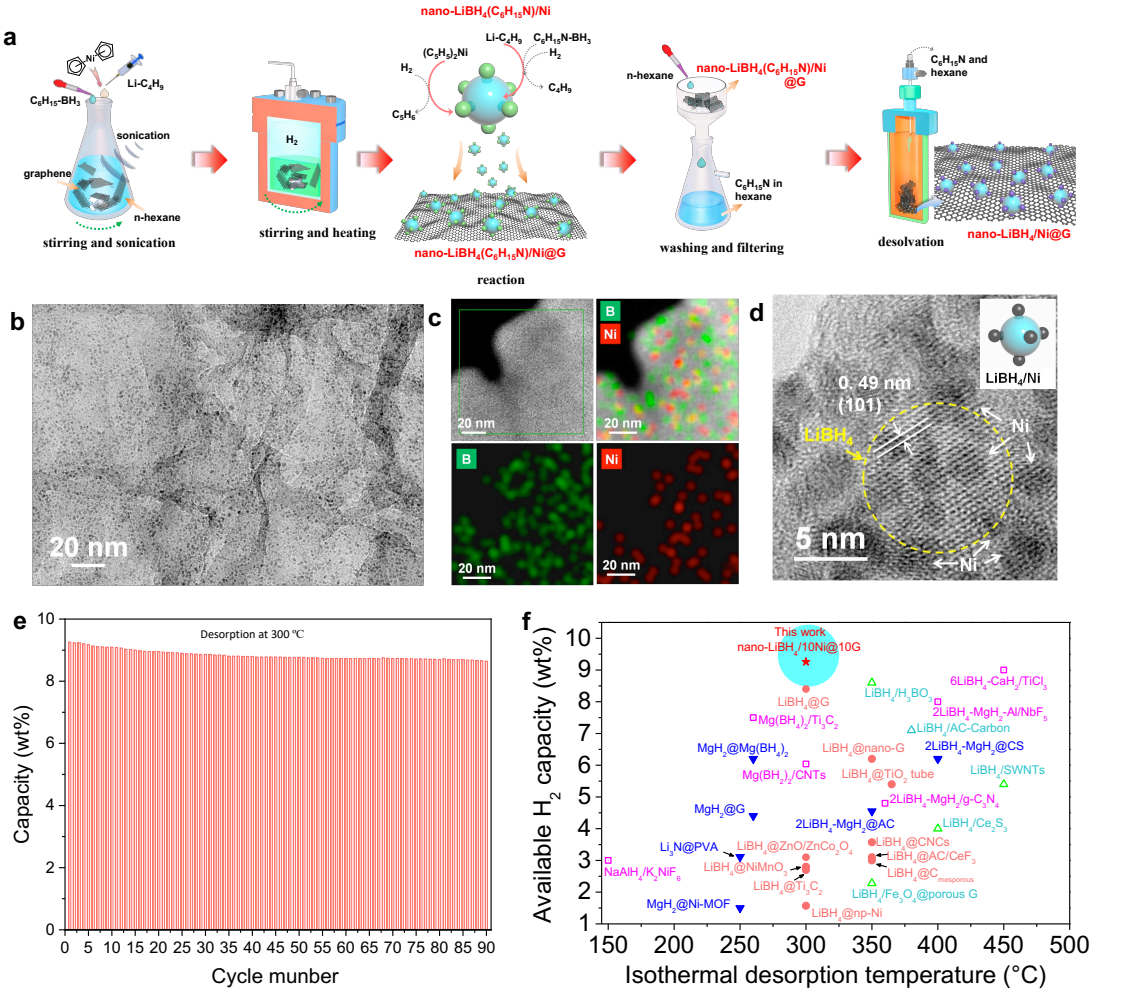

Figure 11 (a) Schematic illustration of the preparation process, (b) TEM image, (c) EDS mapping, (d) HRTEM image, and (e) cycling stability of nano-$LiBH_4$/Ni@G composite. Comparison of isothermal dehydrogenation performance of nano-$LiBH_4$/Ni@G with other hydride-based hydrogen storage materials (f). Reproduced with permission.[140] Copyright 2021, Elsevier.

Table 1 Hydrogen storage properties of $LiBH_4$-based reactive destabilization systems

System	H capacity (wt%)	T_{onset} (°C)	ΔH (kJ mol^{-1} H_2)	Reaction	Ref.
$2LiBH_4$-MgH_2	8.0-10.0	270	40.5	$LiBH_4 + 1/2MgH_2 \rightarrow LiH + 1/2MgB_2 + 2H_2$	[41]
$2LiBH_4$-Mg	5.6			$2LiBH_4 + Mg \rightarrow MgB_2 + 2LiH + 3H_2$	[43b]
$2LiBH_4$-Al	8.5		18.8	$2LiBH_4 + Al \rightarrow AlB_2 + 2LiH + 3H_2$	[43d]
$LiBH_4$-$LiAlH_4$	8.7	138		$LiBH_4 + LiAlH_4 \rightarrow 3/2LiH + 1/2LiAl + 1/2AlB_2 + 13/4H_2$	[43e]
$6LiBH_4$-CaH_2	9.1	150	59.2	$6LiBH_4 + CaH_2 \rightarrow 6LiH + CaB_6 + 10H_2$	[43f]
$LiBH_4$-0.58$LiAlH_4$-$32MgH_2$	7.62	280	78±8.86	$32MgH_2 + 0.58LiAlH_4 + LiBH_4 \rightarrow 0.25MgAlB_4 + 0.0275Mg_{17}Al_{12} + 0.53Li_3Mg_7 + 27.6Mg + 35.2\ H_2$	[43g]
$2LiBH_4$-Mg_2FeH_6	7.45	217	72	$4LiBH_4 + 2Mg_2FeH_6 \rightarrow MgB_2 + 4LiH + 12H_2 + 2FeB + 3Mg$	[43h]
$LiBH_4$-$1/2Mg(AlH_4)_2$	10.8	60		$LiBH_4 + 1/2Mg(AlH_4)_2 \rightarrow 1/4MgAlB_4 + 3/8LiAl + 1/8Al_3Mg_2 + 5/8LiH + 59/16H_2$	
$LiBH_4$-$1/4Mg(AlH_4)_2$	11.5	89		$LiBH_4 + 1/4Mg(AlH_4)_2 \rightarrow 1/4MgAlB_4 + 1/4Al + 3/4LiH + 21/8H_2$	[43i]
$LiBH_4$-$1/6Mg(AlH_4)_2$	11.8	112		$LiBH_4 + 1/6Mg(AlH_4)_2 \rightarrow 1/6MgAlB_4 + 1/6LiAl + 5/6LiH + 3B + 27/12H_2$	
$LiBH_4$-$2ScH_2$	4.5	280	34.1	$ScH_2 + 2LiBH_4 \rightarrow ScB_2 + 2LiH + 4H_2$	[43k]
$6LiBH_4$-CeH_2	4.6	260	44	$6LiBH_4 + CeH_2 \rightarrow CeB_6 + 6LiH + 10H_2$	[43o]
$6LiBH_4$-LaH_2	5.1	260	70	$6LiBH_4 + LaH_2 \rightarrow LaB_6 + 6LiH + 10H_2$	[43o]
$12LiBH_4$-$2LaH_3$-$17MgH_2$	6.9	225		$12LiBH_4 + 2LaH_3 + 17MgH_2 \rightarrow 2LaB_6 + 12LiH + 17Mg + 38H_2$	[43p]
$LiBH_4$-Li_3AlH_6	8.5	160		$LiBH_4 + Li_3AlH_6 \rightarrow 1/2LiAl + 1/2AlB_2 + 7/2LiH + 13/4H_2$	[43q]
$10LiBH_4$-$Ca(AlH_4)_2$	8.8	150		$10LiBH_4 + Ca(AlH_4)_2 \rightarrow CaB_6 + 2AlB_2 + 10LiH + 19H_2$	[43r]
$6LiBH_4$-CaH_2-$3MgH_2$	8.0	290		$6LiBH_4 + CaH_2 + 3MgH_2 \rightarrow 6LiH + CaB_6 + 3Mg + 13H_2$	[44]
$4LiBH_4$-$5Mg_2NiH_4$	4.8	250	15.4 ± 2	$4LiBH_4 + 5Mg_2NiH_4 \rightarrow 2MgNi_{2.5}B_2 + 4LiH + 8MgH_2 + 8H_2$	[45,46]
$2LiBH_4$-$Ca(BH_4)_2$-$2MgH_2$	8.1	320	40.3	$Ca(BH_4)_2 + 2LiBH_4 + 2MgH_2 \rightarrow 1/3CaH_2 + 2/3CaB_6 + 2LiH + 2Mg + 26/3H_2$	[47]
$12LiBH_4$-Bi_2Te_3	9.0	61		$12LiBH_4 + Bi_2Te_3 \rightarrow 3Li_2Te + 2Li_3Bi + 12B + 24H_2$	[51]
$LiBH_4$ -$2LiNH_2$	10.0	250		$LiBH_4 + 2\ LiNH_2 \rightarrow Li_3BN_2 + 4\ H_2$	[52a]
$Li(NH_3)_{4/3}BH_4$	17.8	135		$Li(NH_3)_{4/3}BH_4 \rightarrow 1/3\ Li_3BN_2 + 2/3\ BN + 4H_2$	[53]

Table 2 Hydrogen storage properties of $LiBH_4$ mixed with catalytic additives.

Catalytic Additives	Addition amount	H capacity (wt%)	T_{onset} (°C)	E_a (kJ mol^{-1} H_2)	Isothermal desorption performance	Ref.
SiO_2	25 wt%	9	~200	156 ± 20		[23]
Fe_2O_3	66.7 wt%	~6	~100			[55a]
V_2O_5	66.7 wt%	~5.5	~100			[55a]
Nb_2O_5	80 wt%	~4	~100			[55a]
TiO_2	80 wt%	~3.5	~100			[55a]
$TiCl_3$	10 mol%	6	100			[55b]
TiF_3	10 mol%	8.5	~100			[55b]
ZnF_2	10 mol%	6	~120			[55b]
$FeCl_2$	50 mol%	~18	~100			[55c]
$CoCl_2$	50 mol%	~12	~100			[55c]
$NiCl_2$	50 mol%	18.3	~100			[55c]
$(Ce,La)(Cl,F)_3$	25 mol%	3.05				[55d]
Ni	33 mol%	17.2	300			[55e]
TiF_4	25 mol%	5.3	65			[56]
Ni supported on graphene	20 wt%	15.2	180		450 °C, 45 min, 12.8 wt% H	[57]
Ni supported by porous carbon	20 wt%	~15	180			[58]
Ti_3C_2 MXene	40 wt%	~9	120	70.3	350 °C, 1h, 5.37 wt% H	[60a]
Ce_2S_3	20 wt%	~7	250	157.82	400 °C, 3000 s, 4.0 wt% H	[60b]
$NiFe_2O_4$	7 mol%	10.84	88			[60c]
As-prepared single-walled carbon nanotubes	30 wt%	12.3	280			[61]
Single-walled carbon nanotubes	30 wt%	12.3			450 °C, 90 min, 10 wt% H	[62]
Activated carbon	30 wt%	11.2			450 °C, 90 min, 10 wt% H	[62]
Graphite	30 wt%	9.9			450 °C, 90 min, 6.5 wt% H	[62]
Multi-walled carbon nanotubes	64 wt%	~5.5	210			[63]
Graphene	20 wt%	11.4	230	40	450 °C, 90 min, 9.2 wt% H	[65]
Three-dimensional porous Fluorinated graphene	20 wt%	10.01	204	130.87	400 °C, 1000 s , 3.45 wt% H	[66]
Porous Li_3BO_3	33 wt%	~8	105		450 °C, 2000 s, 4.12 wt% H	[69]
Li_3BO_3-NbH	6 mol%	6.8	180	127.4	400 °C, 60 min , 6.8 wt% H	[70]

Table 3 Hydrogen storage properties of nanoconfined $LiBH_4$ systems

Scaffolds	T_{onset}/T_{peak} (°C)	H Capacity (wt%)	E_a (kJ mol^{-1} H_2)	Isothermal desorption performance	Method	Ref.
Nanoporous carbon scaffolds	230/381	3.7	103±4	300 °C, 12.5 wt% h^{-1}	melt impregnation (280-300 °C)	[73]
Mesoporous carbon	200/335	6.0	-	300 °C, 90 min, 3.4 wt% H	MTBE assisted wet impregnation	[74]
Carbon nanotubes	75/-	0.27 ± 0.05	88±5		THF assisted wet impregnation	[75]
Highly ordered nanoporous carbon	220/342	7.5	-	-	melt impregnation (300°C, 60 bar, 30 min)	[76,77]
Activated carbon nanofiber	272/357	11.7 (referred to $LiBH_4$)	-	-	melt impregnation (350 °C, 80 bar, 12 h)	[78]
PMMA-co-BM polymer matrix	80/105	8.8 (referred to $LiBH_4$)		120 °C, 4 h, 0.74 wt% H	THF assisted wet impregnation	[79]
Porous hollow carbon nanospheres	200/356	8.3	93.9-129.7	350 °C, 25 min, 8.1 wt% H	melt impregnation (300 °C, 100 bar, 30 min)	[80]
Cu-MOFs	75/110	0.0048 mol g^{-1}			Ether assisted wet impregnation	[81]
Carbon nanocages	200/320	7.18	113.5	350 °C, 2250 s, 3.57 wt% H	melt impregnation (310 °C , 60 bar , 2 h)	[82]
Zeolite-templated carbon	194/336	13.4 (referred to $LiBH_4$)	129.0	300 °C, 33.3 wt % h^{-1}	melt impregnation (300 °C , 140 bar , 30 min)	[83]
Ordered mesoporous silica (SBA-15)	45/92	~11 (referred to $LiBH_4$)	545	105 °C, 10 min, 8.5 wt% H	THF assisted wet impregnation	[84]
Double-layered carbon nanobowl	225/353	10.9	121.4	300 °C, 82.4 wt % h^{-1}	melt impregnation (300 °C , 100 bar , 5-30 min)	[85]
Porous TiO_2 micro-tubes	183/291	14.715	121.9	310 °C, 1 h, 2.47 wt% H	THF assisted wet impregnation	[86a]
Porous $NiMnO_3$ microspheres	150/300	7.3	129.8	300 °C, 1 h, 2.8 wt% H	THF assisted wet impregnation	[86b]
Hierarchical Pporous $ZnO/ZnCo_2O_4$ nanoparticles	169/275	8.7	120.22	300 °C, 60 min, 3.4 wt% H	THF assisted wet impregnation	[86c]
Ti_3C_2	176.2/278.4,322.8	11.3	94.44	380 °C, 1 h, 9.6 wt% H	THF assisted wet impregnation	[86d]
Graphene	~200/346	~12	119.6	340 °C, 60 min, 9.7 wt% H	thermal treatment (120 °C, 3 days)	[87]

Table 4 Hydrogen storage properties of catalyst-modified $2LiBH_4$-MgH_2 system

Catalytic Additives	Addition amount	H Capacity (wt%)	T_{onset} (°C)	E_a (kJ mol^{-1})	Ref.
$TiCl_3$	2-3 mol%	8-10			[41]
$TiCl_3$/ $HfCl_4$/ $ZrCl_4$/ VCl_3	3 mol%		260		[88]
$TiCl_3$	5 mol%	6-7	240		[88]
$NiCl_2$	10 mol%	9.4	~275	119.5 ± 6.9 (MgH_2), 116.1 ± 3.8 ($LiBH_4$)	[89]
NbF_5	5 mol%	8.1	350		[90a]
NbF_5	9 wt%	8.31	~360		[90c]
TiF_4	10 mol%	>9			[93b]
TiB_2/ NbB_2	5 mol%	10		101.2-116.2 (MgH_2), 104.6-105.1 ($LiBH_4$)	[94]
CoNiB	10 wt%	10.8	180	137 (MgH_2), 116 ($LiBH_4$)	[95]
Pd	9 wt%	8.0	260		[97]
Ru supported on multiwalled carbon nanotubes	20 wt%	11	250-300		[98]
Fe	10 mol%	7	300		[99]
Nb_2O_5	16 wt%	7.4	~200	139.96 (MgH_2), 156.75 ($LiBH_4$)	[101]
Fe_2O_3+TiF_3	10 wt%	9.6	110		[104]
$BaTiO_3$	20 wt%	7.48	299	138.54	[105]
Single-walled carbon nanotubes	10 wt%	10	~300		[108]
multi-walled carbon nanotubes (MWCNTs)	$LiBH_4$:MWCNTs =1:1	12	250		[110]
multiwall carbon nanotubes decorated with TiO_2	15 wt%	6.8	355		[112]

Table 5 Hydrogen storage properties of nanoconfined thermodynamically destabilized systems

System	Scaffolds	H Capacity (wt%)	T_{onset} (°C)	E_a (kJ mol^{-1})	Isothermal desorption performance	ΔH (kJ mol^{-1} H_2)	Method	Ref.
$2LiBH_4$ - MgH_2	nanoporous carbon aerogel scaffold	4.7	~260	-	390 °C, 20 h, 3.9 wt%		MgH_2 impregnation and $LiBH_4$ melt infiltration	[114]
$2LiBH_4$ - MgH_2	nanoporous resorcinol-formaldehyde carbon aerogel scaffold	3.5	2~250	-	425 °C, 90 min, 90% of total capacity		melt impregnation (310°C, 60 bar, 90 min)	[115]
$2LiBH_4$-MgH_2	Resorcinol-formaldehyde aerogel scaffolds	3.6	250-300	89±2 (MgH_2), 279±5 ($LiBH_4$)	-	46.21	MgH_2 impregnation and $LiBH_4$ melt infiltration (310°C, 60 bar, 30 min)	[116]
$2LiBH_4$-MgH_2	Carbon aerogel scaffold	3.9	200	124.8 (MgH_2), 124.8($LiBH_4$)	320 °C, 2 h, 4.54 wt%		melt infiltration (310°C, 64 bar, 30 min)	[117]
$2LiBH_4$-MgH_2	Graphene	9.1	235	-	400 °C, 40 min, 9.1wt%	39.2	solvothermal treatment, wet impregnation with THF as solvent	[118]
$LiBH_4$–Mg_2NiH_4	templated carbon	3.4	100		450 °C, 1.6 h, 3.8 wt%		melt infiltration (300°C, 100-150 bar, 30 min)	[120]
	carbon aerogel	4.2	200				melt infiltration (300°C, 100-150 bar, 30 min)	[120]
$LiBH_4$-$LiAlH_4$	Activated carbon nanofiber	4.8	220	-	-	-	wet impregnation with THF and diethyl ether as solvent	[121]

$2LiBH_4$-$NaAlH_4$	Mesoporous carbon aerogel scaffold	2.48	<100	-	-	-	melt infiltration (310°C, 110 bar, 30 min)	[122]
$LiBH_4$–MgH_2–$NaAlH_4$	carbo n aerogel scaffold	3.0	150	-	-	-	melt infiltration (310°C, 100 bar, 45 min)	[123]
$0.68LiBH_4$-$0.32Ca(BH_4)_2$	Mesoporous Carbon	5	230	-	-	-	melt infiltration (230°C, 3 bar, 30 min)	[124,125]
$0.7LiBH_4$−$0.3Ca(BH_4)_2$	CO_2-activated carbon aerogel scaffolds	7.71	243	130	270~331 , ℃ 6.8 wt%		melt infiltration (230°C, 110-130 bar, 30 min)	[126]
	carbon aerogel scaffolds	3.36	~150	156	270~331℃, 3 wt%			
$0.62LiBH_4$-$0.38NaBH_4$	carbon aerogel scaffolds	3.95	~200	116-118	-	-	melt infiltration (240°C, 140-168 bar, 30 min)	[127]
$0.725LiBH_4$-$0.275KBH_4$	mesoporous CMK-3 type carbon	6.7	177	-	-	-	melt infiltration (125°C, 100 bar, 30 min)	[128]
$0.55LiBH_4$-$0.45Mg(BH_4)_2$	nanoporous carbon aerogels	2.68	~150				melt infiltration (190°C, 110-130 bar, 30 min)	[129]
	CO_2-activated carbon aerogel scaffolds	7.64	~200					
$LiBH_4$-$Mg(BH_4)_2$	hollow carbon nanospheres	12	~200	165.1 ± 2.8	280 ℃, 300 min, 10.8 wt%		melt infiltration (190°C, 60 bar, 1 h)	[130]

Table 6 Hydrogen storage properties of nanoconfined $LiBH_4$-based systems with various additives

System	Scaffolds	Catalytic Additives	H Capacity (wt% H_2)	T_{onset}/T_{peak} (°C)	E_a (kJ/mol)	Isothermal desorption performance	Method	Ref
$LiBH_4$	porous carbon	Ni	10 (referred to $LiBH_4$)	200/350		400 °C, 25 min, 3.5 wt%	melt infiltration	[132, 133]
$LiBH_4$	activated carbon nanofibers	TiO_2	5.2	~260/359			melt infiltration	[134]
$LiBH_4$	active porous core–shell network structure	TiO_2	9.8	220/316	91.56	320 °C, 60 min, 7.3 wt%	melt infiltration	[135]
$LiBH_4$	Reduced graphene oxide (rGO) modified melamine foam	poly(methylmethacrylate)	11	94/-		250 °C, 25 min, 2.9 wt%	wet impregnation	[136]
$LiBH_4$	carbon aerogels	CoNiB	15.9	192/320	46.39	350 °C, 30 min, 9.33 wt%	wet impregnation	[137]
$LiBH_4$	activated carbon	CeF_3	12.8	160-180/320.1-326.2	108	350 °C, 500 s, 11.8 wt%	melt infiltration	[138]
$LiBH_4$	graphene	Ni	11.6	130/285	106	200°C, 600 min, 7.5 wt%	solvothermal process	[140]
$2LiBH_4$-MgH_2	carbon aerogel	$TiCl_3$	3.58	250/277		425 °C, 2 h, 3.5 wt%	melt infiltration	[141a]
$2LiBH_4$-MgH_2	carbon aerogel	$TiCl_4$	3.4	140/		425 °C, 0.5 h, 3.6 wt%	melt impregnation	[141b]
$2LiBH_4$-MgH_2	carbon aerogel	$ZrCl_4$	5.4	200/		425 °C, 5 h, 3.7 wt%	melt impregnation	[141c]

This review covers the recent development of $LiBH_4$-based materials for hydrogen storage. Effective strategies for tailoring thermodynamics and kinetics of hydrogen cycling processes are summarized, including cation/anion substitution, reactive compositing, catalyst doping and nanoengineering. The challenges and the directions of future research are also analyzed and discussed.

Keywords: hydrogen, hydrogen storage, borohydrides, $LiBH_4$, thermodynamics, kinetics

*Wenxuan Zhang, Xin Zhang, Zhenguo Huang, Haiwen Li, Mingxia Gao, Hongge Pan, Yongfeng Liu**

Recent Development of Lithium Borohydride-based Materials for Hydrogen Storage

ToC figure